Solid State Lithionics based Ethylene Gas-Sensing and Ionic Decision Maker Devices

M.Sc. Thesis

By Sahin Gazi



DEPARTMENT OF CHEMISTRY INDIAN INSTITUTE OF TECHNOLOGY INDORE

MAY 2025

Solid State Lithionics based Ethylene Gas-Sensing and Ionic Decision Maker Devices

A THESIS

Submitted in partial fulfillment of the requirements for the award of the degree

of

Master of Science

By
Sahin Gazi



DEPARTMENT OF CHEMISTRY INDIAN INSTITUTE OF TECHNOLOGY INDORE

MAY 2025



CANDIDATE'S DECLARATION

I hereby certify that the work which is being presented in the thesis entitled "Solid State Lithionics based Ethylene Gas-Sensing and Ionic Decision Maker Devices" in the partial fulfillment of the requirements for the award of the degree of MASTER OF SCIENCE and submitted in the DEPARTMENT OF CHEMISTRY, Indian Institute of Technology Indore, is an authentic record of my own work carried out during the time period from July 2024 to May 2025 under the supervision of Dr. Pravarthana Dhanapal, Assistant Professor, Department of Chemistry, IIT Indore. The matter presented in this thesis has not been submitted by me for the award of any other degree of this or any other institute.

Sahin Gazi 19/05/2025

Signature of the student with date (Sahin Gazi)

This is to certify that the above statement made by the candidate is correct to the best of my/our knowledge.

Signature of Thesis Supervisor with date (Dr. Pravarthana Dhanapal)

Sahin Gazi has successfully given his M.Sc. Oral Examination held on 15

th May, 2025.

Signature of Supervisor M.Sc. thesis

ACKNOWLEDGEMENTS

This is a great chance for me to express my gratitude to everyone who has supported me during my M.Sc. project. I would like to express my special thanks to my supervisor **Dr. Pravarthana Dhanapal** for all of his help, support, and advice during my M.Sc. project. Under whose guidance I have accumulated valuable experience and learned some aspects of Solid-State Chemistry and Solid-State Ionic Device. His valuable input has helped me learn many skills that have been very fruitful throughout my research experience. I would also want to take this opportunity to thank our esteemed Director, **Prof. Suhas Joshi** and **Prof. Tushar Kanti Mukherjee**, Head of the Chemistry Department at IIT Indore, for providing the environment and infrastructure needed to conduct research. Additionally, I want to express my gratitude to the entire faculty of IIT Indore and SIC for consistently showing a supporting gesture.

I am grateful to **Prof. Vinod Kumar**, Department of Metallurgical Engineering and Material Science for his lab facilities, **Prof. Somaditya Sen**, Department of Physics for the XRD facility, **Dr. Girish Chandra Verma**, Department of Mechanical Engineering for the Autolab Metrohm facility.

I am thankful to Mr. Pranjal Shrimali, Mr. Shubham Verma, Mr. Mahesh Chand Bairwa, Mr. Gokul Pillai, Department of Metallurgical Engineering and Material Science for their technical support and assistance throughout the year. Also, I would like to thank all the lab members of Dr. Pravarthana Dhanapal's research group for their support and work.

Most significantly, without the support of my family members, it would have been impossible for me to reach here.

I want to thank my parents, friends, and seniors for their support and encouragement throughout my life, for lifting my spirits during the difficult moments of this journey and for consistently showing support and understanding.

Sahin Gazi

Department of Chemistry

IIT INDORE

DEDICATED TO MY FAMILY AND FRIENDS



ABSTRACT

In recent years, pollution and environmental hazards have been the main problem globally. Pollution damages the environmental ecosystem. The prevalence of many diseases is rising due in large part to pollution, which affects human health in many ways. The gas sensing devices are very important for monitoring the environmental ecosystem and reducing harmful gases to save our lives. Developing an ethylene gas sensor is very important to solve the spoilage of fruits and save the economic losses, estimated at billions of dollars annually in the agriculture sector and food industry. The development of an ethylene gas sensor and the impact of doping on its characteristics are the main objectives of this project. We have used in-situ doping into WO3 to modify the Li-ion concentration via solid state ionics. The sensor's effectiveness has been demonstrated through tests using ethylene gas. My second objective, decision-making is frequently performed in the areas of computation to get better results in a wide variety of current intelligence activities. The decision-maker device is able to solve different multi-armed bandit problems (MBPs). The ionic decision-maker device also mimics the decision-making process of the human brain. A neural network is developed in our human brain by billions of neurons. Our decision-maker device can predict the image of this neural network data and make decisions. By changing Li ion concentration via solid state Ionics by in-situ doping into WO₃, the decision maker device will be developed. Brain-inspired neuromorphic computing is a revolutionary technology to create an intelligent and energy-efficient computing system. Here, we propose a three terminal artificial synaptic ionic decision-maker device based on ion movement. The WO₃ based artificial synapse shows synaptic behaviors including excitatory postsynaptic current and pairedpulse facilitation as short-term plasticity. The artificial synapse emulates the

transition characteristics of a biological synapse from short-term to longterm plasticity depending on the amplitudes of the applied bias pulses.

TABLE OF CONTENTS

1.	List of F	X11-X1V		
2.	Acronyn	XV		
3.	Chapter	1		
	1.1 Solid state ionics		1-4	
	1.2	1.2 Ethylene gas sensing		
	1.3	Challenges in ethylene gas sensing	6-7	
	1.4	Biological neural driven by ionics	7-10	
	1.5	Multi armed bandit problems (MBPs)	10-11	
	1.6	Focus of the work	11-12	
	1.7	Methodology	12-14	
4.	Chapter	2: Literature Review	15-20	
5.	Chapter	3: Objectives	21-22	
6.	Chapter	4: Experimental section	23	
	4.1	Materials used	23	
	4.2	Chemicals required	23	
	4.3	Device fabrication and experimental set u	ip 23-29	
7.	Chapter	5: Results and discussion	30	
	5.1	Characterization of LLZO powder and sin	ntered LLZO	
powde	r		30-32	
	5.2	Ethylene gas sensing study of the device	32-42	
	5.3	Synaptic behaviours study of the device	42-48	
	5.4	Characterization of WO ₃ film on LICGC	48-51	
	5.5	Gas sensing mechanism	51-52	
8.	Chapte	r 6: Conclusion	53	
9	. Chapte	er 7: Future scope	54	

References

55-59

LIST OF FIGURES

- Figure 1: Various solid state ionic devices operated by utilizing ion transport and electrochemical phenomena in solids [5].
- Figure 2: Challenges and perspectives of lithium-ion transport in solid-state electrolyte [6].
- ➤ **Figure 3:** Schematic illustration of comparing electronic devices, conventional material synthesis, and nanoionic devices.
- Figure 4: Fruit ripening is happened by ripening hormone ethylene.
- ➤ **Figure 5:** Energy diagram at the solid electrolyte-semiconductor interface [13].
- > Figure 6: Challenges in ethylene gas sensing
- ➤ Figure 7: Biological neural systems. (a) Schematic structure of biological neural systems consisting neurons and synapses ^[15]. (b) signal transmission across the cell membrane ^[12]. (c) Synaptic properties, including various learning and forgetting functions ^[13].
- Figure 8: (A) 1: Illustration of MBP. Gambler selects and plays slot machines to maximize total reward. 2: MBP in the channel model, in which a communication network user attempts to select an available channel [18].
- > Figure 9: Different types of gas sensor device.
- Figure 10: Advantages of synaptic devices and their applications in biomimetic sensory neural systems [35].
- Figurer 11: (a) Schematic diagram of gas sensing device. (b) top view of gas sensing device.
- Figure 12: (a) Schematic diagram of artificial synaptic ionic decision-making device. (b) top view of artificial synaptic ionic decision-making device.
- Figure 13: Schematics diagram Al-doped LLZO pellet formation.

- Figure 14: Schematic diagram of a Spark Plasma Sintering equipment.
- Figure 15: Schematic layout of a typical DC magnetron sputtering unit.
- Figure 16: (a) The experimental circuit set up for the I-V measurement of synaptic device. (b) Picture of the Keithley instrument.
- > Figure 17: Gas sensing circuit set up
- Figure 18: XRD data of (a) pure Al-doped LLZO powder (b) sintered LLZO powder.
- Figure 19: (a) TGA data of pure Al-doped LLZO powder (b) TGA data of sintered Al-doped LLZO powder.
- Figure 20: Ethylene gas sensing curves for 2 and 3 ppm of gas at an operating temperature of 50 °C.
- ➤ Figure 21: Ethylene gas sensing curves for 3 ppm of gas (a) at an operating temperature of 50 °C and constant bias voltage -5 V (b) at an operating temperature of 50 °C and constant bias voltage 5 V (c) at an operating temperature of 60 °C and constant bias voltage 7 V (d) at an operating temperature of 80 °C and constant bias voltage 5 V.
- ➤ Figure 22: Ethylene gas sensing curves for 3 ppm of gas (a) at an operating temperature of 100 °C and constant bias voltage 10 V (b) at an operating temperature of 120 °C and constant bias voltage 10 V (c) at an operating temperature of 150 °C and constant bias voltage 5 V (d) at an operating temperature of 170 °C and constant bias voltage 5 V.
- Figure 23: Ethylene gas sensing curves for 3 ppm and 5 ppm of gas at room temperature of 25 °C and (a) constant gate voltage -2 V (b) constant gate voltage -1 V (c) constant gate voltage -0.5 V (d) constant gate voltage 0 V. (e) constant gate voltage 1 V (f) constant gate voltage 2 V.

- Figure 24: (a) and (b) Drain current change during V_G sweep of the device at constant V_D = 0.5 V (c) Gate current change during V_G sweep of the device (d) Drain current change during V_D sweep of the device at different V_G.
- Figure 25: Potentiation–depression curves of synaptic device at constant drain voltage $(V_D) = 0.5 \text{ V}$ and at same off gate voltage $(V_G, OFF) = 0.3 \text{ V}$, at $V_{G, ON}$ voltage (a) 0.5 V (b) 1 V (c) 1.5 V (d) 2 V respectively.
- Figure 26: Potentiation—depression curves of synaptic device at constant drain voltage (V_D) = 0.5 V and at same on gate voltage (V_G, o_N) = 2 V, at V_G, o_{FF} voltage (a) -1 V (b) -0.5 V (c) 0.5 V (d) 1 V respectively.
- ➤ Figure 27: (a) The XRD data of deposited WO₃ film on LICGC (b)

 The Raman data of deposited WO₃ thin film on LICGC substrate.
- ➤ Figure 28: FE-SEM micrographs for the deposited WO₃ film on LICGC substrate at (a) 2.04 KX(b) 5.49 KX (c) 20.33 KX magnification.
- Figure 29: AFM images of the film taken in a 10x10 micron area taken in (a) 0.5 Hz scan rate (b) 1 Hz scan rate.
- Figure 30: A schematic representation of an n-type chemiresistor gas sensor [42].

ACRONYMS

PXRD Powder X-Ray Diffraction

SEM Scanning Electron Microscopy

AFM Atomic Force Microscopy

TGA Thermogravimetric Analysis

MBPs Multi Armed Bandit Problems

LTP Long Term Potentiation

STP Short Term Potentiation

LLZO Lithium Lanthanum Zirconium Oxide

LICGC Lithium-Ion Conductive Glass Ceramics

PLD Pulsed Laser Deposition

PVA Polyvinyl Alcohol

IPA Isopropyl Alcohol

Chapter 1: Introduction

1.1 Solid state ionics:

In the classical Greek language, the phrase "ion" stands for "going" or "moving" [1]. Ions are electrically charged species that possess either positive or negative charges. The term ionics deals with the movement of ions, which can occur due to concentration gradient or under external driving forces such as an electric field. The application of ionics is vast, ranging from biological systems, batteries, fuel cells, and neuromorphic computing [2]. Systems like neuromorphic transistors and biological synapses can be operated efficiently and modulated by ionics [3]. The phenomena of ionics can occur in various states of matter. Solid-state ionic is a multi-disciplinary research field which combines physics, chemistry, and material science. The term "Solid State Ionics" was first introduced by Takahashi in 1972 fall meeting of the American Electrochemical Society [4]. An international journal named "Solid State Ionics" has been published continuously since 1980. In particular, solid-state ionic devices operated by ions movement and electrochemical redox reactions like oxidation and reduction facilitate various advantages such as easy integration with existing technology platforms, miniature devices, and low power consumption. This field explores how ions move through solid electrolytes and the mechanisms that govern this movement, which are crucial for various applications such as batteries, fuel cells, actuators, etc. The solidstate ionic approach has extensively advanced for various applications like the field of electronics using electrons conduction. Rechargeable batteries, gas sensor devices, actuators, memristive devices, decision maker devices, artificial perception, and electrochromic devices are developed using solidstate ionics, that mainly operate on ion movement and electrochemical redox reactions ^[5]. Typical devices of this type are shown in Figure 1.

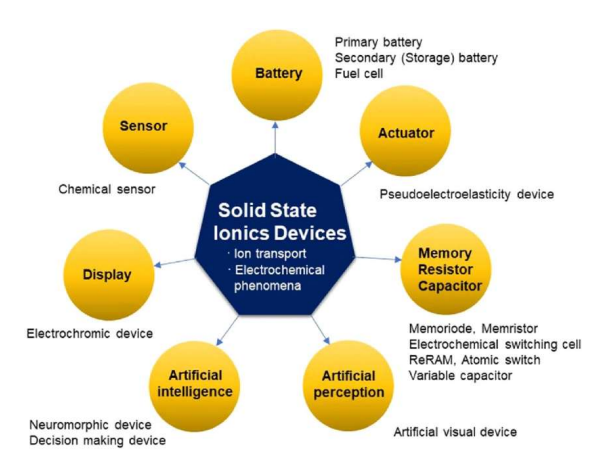


Figure 1: Various solid state ionic devices operated by utilizing ion transport and electrochemical phenomena in solids ^[5].

The shift from large, power-hungry devices to affordable, low-power consuming solid state devices has been made feasible by the concurrent developments in the semiconductor industry, material science, and thin film technologies. The solid-state ionic approach has extensively advanced for various applications like the field of electronics using electrons conduction. The solid-state ionic device provides various advantages, such as high thermal stability, high energy density, and high selectivity compared to liquid-state technologies/devices.

Since solid-state Li-based batteries have advanced so quickly in recent years, the industrial and academic communities have made a lot of efforts to improve solid-state electrolyte performance. The discovery of the lithium-ion battery is a landmark achievement in electrochemistry and materials science, enabling the modern era of portable electronics, electric vehicles, and energy storage. There were multiple reasons for choosing lithium-ion in batteries. It is the 3rd lightest element in the periodic table, and has a small ionic radius thus a high diffusion coefficient. However, before being used on a big basis, a number of issues must be resolved in contrast to commercial liquid electrolytes. Among these difficulties are

strategies to improve bulk Li-ion transport, reduce grain boundary resistance at the solid electrolyte-electrode interface, and strengthen the durability of the solid-state electrolyte structure and interface over extended cycling as shown in figure 2 [6].

Lithium-ion transport in solid-state electrolyte

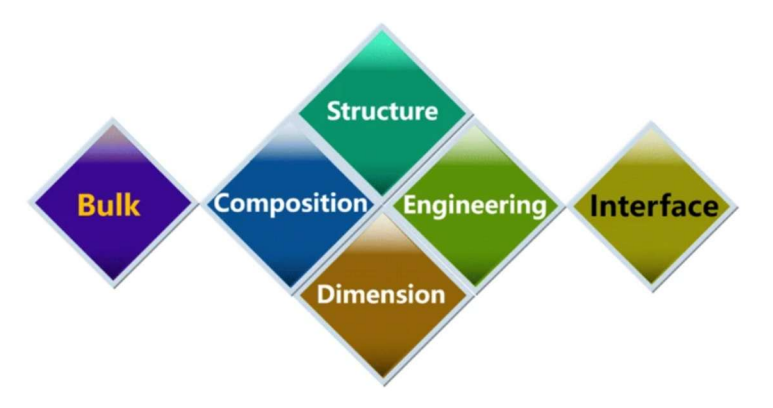


Figure 2: Challenges and perspectives of lithium-ion transport in solid-state electrolyte ^[6].

The following benefits make this research useful for gas sensing and artificial synaptic based ionic decision-maker applications of solid state ionics-based devices.

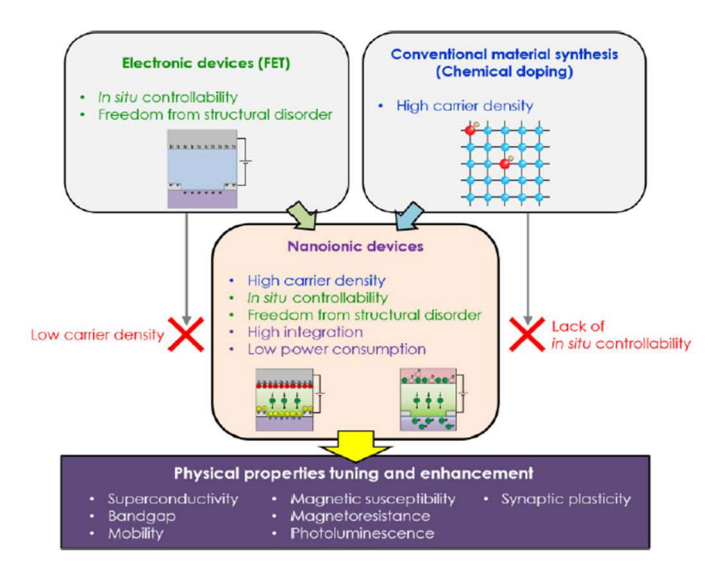


Figure 3: Schematic illustration of comparing electronic devices, conventional material synthesis, and nanoionic devices.

1.2 Ethylene gas sensing:

In recent years, pollution and environmental hazards have been the main problem globally. Pollution damages the environmental ecosystem. The prevalence of many diseases is rising due in large part to pollution, which affects human health in many ways. The field of gas sensing is very important for monitoring the environmental ecosystem and reducing harmful gases to save our lives. A gas sensor device is a transducer that identify gases and generate an electrical signal whose intensity correlates with the gas concentration. The detection of gases primarily involves chemical processes, whereas converting this detection into a signal involves physical processes. Ethylene is a plant ripening hormone as shown in figure 4. It is also responsible for plant growth, organ senescence, and seed germination. When fruit ripening happens, the amount of ethylene gas increases. So, the detection of fruit ripening in exact time is very important.

Developing an ethylene gas sensor is very important to solve the spoilage of fruits and save the economic losses, estimated at billions of dollars annually in the agriculture sector and food industry. The agricultural sector significantly contributes to the GDP, making up approximately 5,688 billion rupees, or nearly 21% of the total. This sector serves as the primary source of income for 55% of the population. The ethylene gas sensor device also operates at very high temperatures. Efficient ethylene gas sensing needs to be done for spoilage of fruits in storage containers or cold storage. The different metal oxides like MnO₂, V₂O₅, WO₃, and ZnO are promising for ethylene gas sensing. In metal oxides, the depletion region is present due to oxygen vacancies, resulting in metal oxide exhibiting n-type conductivity.

For detecting gases, the depletion region plays a major role. The depletion region is formed at the interface of solid electrolyte and metal oxide surface as shown in figure 5 [7]. Semiconducting metal oxide-based gas sensors are chemiresistive, i.e., resistance will be changed by gas absorption [8]. When oxygen molecules are exposed to air, Oxygen molecules interact with electrons which are present in conduction band of semiconductor metal oxide to form absorbed oxygen or oxide ion. So, the electrons will decrease and the thick depletion region is formed in the surface. Hence, resistance increases and conduction decreases due to thick depletion region. When ethylene gas is introduced into picture, the absorbed oxygen or oxide ion reacts with ethylene gas to form acetaldehyde and electron is returned to conduction band of semiconductor metal oxide. Hence, the thickness of depletion region decreases and the resistance also decreases. So, conduction increases. However, such gas sensing in metal oxide systems occurs at generally temperatures greater than 200 °C. In this regard, highly sensitive ethylene gas using metal oxide systems ranges must be designed to function at room temperature or cold storage temperature of fruits/vegetables of interest, ranging from 0 °C to 25 °C depending on fruits/vegetables.

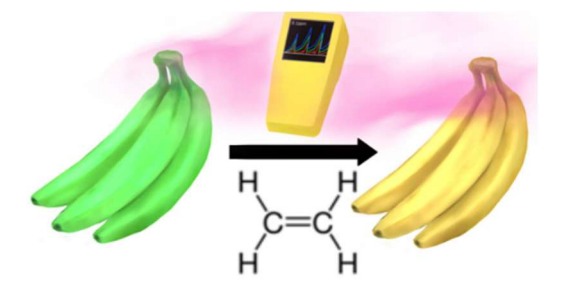


Figure 4: Fruit ripening is happened by ripening hormone ethylene.

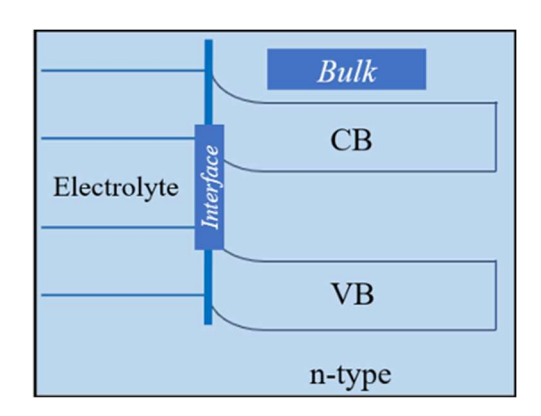


Figure 5: Energy diagram at the solid electrolyte-semiconductor interface [7].

1.3 Challenges in ethylene gas sensing:

The fundamental hydrocarbon molecule ethylene, or C₂H₄, has important functions in the natural world. Its few functional characteristics make it difficult to identify with great sensitivity. Its small molecular size and limited reactivity make things even more challenging. The development of extremely sensitive sensors to identify ethylene is therefore a significant task. To find ethylene, several techniques have been employed ^[9].

The creation of an affordable ethylene gas sensor with adjustable characteristics is our main goal.

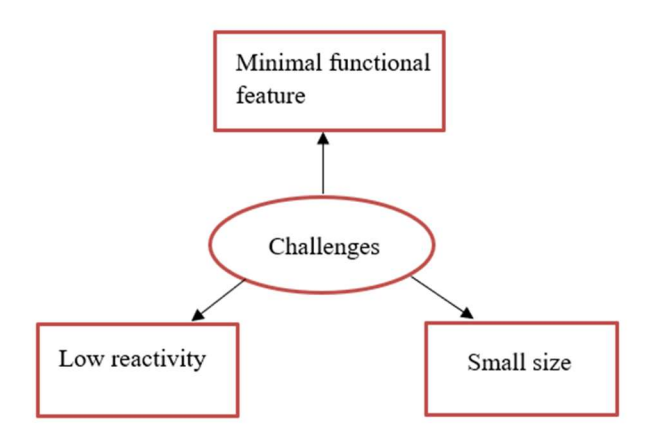


Figure 6: Challenges in ethylene gas sensing.

1.4 Biological neural system driven by ionics:

The focus of this project is on 2 main devices namely gas sensing and artificial synaptic based ionic decision maker. The brain combines various types of cells, but the primary functional unit is a cell called a neuron. The human nervous system is a highly complex neural network. It consists of the peripheral nervous system (PNS) and central nervous system (CNS), working together to facilitate communication between the body and the external environment. The PNS comprises specialized receptors distributed through the eyes, ears, and skin that provide sensory functions such as vision, hearing, touch, etc. Upon detecting these stimuli, sensory in formation is transmitted to the CNS for high-level processing, which undergoes a series of steps, including encoding, transmission, processing, and response. At the core of the biological nervous system, neurons and synapses form the basis of neural communication, enabling the complex processing of information and the coordination of various functions. Figure

7a illustrates the morphology of a typical biological neuron, which mainly has three parts:

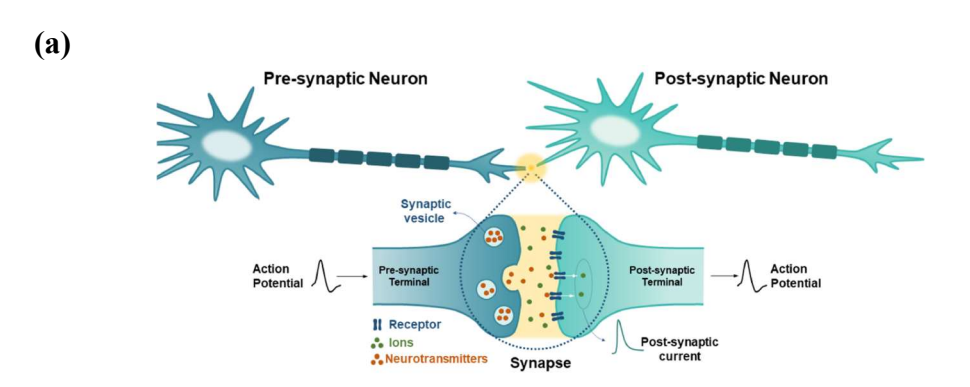
Dendrite to receive input from other neurons, cell body (soma) to process the received information, and axon to deliver processed information to other neurons ^[10]. The connection part of neighboring neurons is called the synapse. One neuron is generally wired with $\approx 10^3$ neurons, and there are $\approx 10^{11}$ neurons and 10^{14} synapses in the brain ^[11]. Synapses are crucial for the transmission of electrical or chemical signals, enabling the flow of information throughout neural networks in the brain.

1.4.1 Biological synapses:

In biological system, the signal from one neuron to another is transmitted via a specialized junction between two neurons called synapse. Synapses are important connections between neurons that enable information communication with in the brain. They are composed of a presynaptic terminal, which releases neurotransmitters, and a postsynaptic terminal, which receives these neuro transmitters. When an action potential reaches the presynaptic terminal, it triggers the opening of voltage-gated calcium channels. As shown in Figure 7b, the influx of calcium ions into the presynaptic terminal facilitates the fusion of synaptic vesicles containing neurotransmitter molecules with the presynaptic membrane. Synapses are crucial for the transmission of electrical or chemical signals, enabling the flow of information throughout neural networks in the brain [12], and the strength of the synapse (synaptic weight) decides the connection strength between two neurons, which can be altered by neural activities. This process is known as synaptic plasticity and is believed to be the backbone of human learning ability and memory. It is necessary to create devices that can mimic the basic processes of biological synapses in order to produce neuromorphic systems.

1.4.2 Synaptic plasticity:

The strength of the synapse (synaptic weight) decides the connection strength between neurons, which can be altered by neural activities in response to action potentials. This process is known as synaptic plasticity and is believed to be the backbone of human learning ability and memory. It includes potentiation/depression long term short-term potentiation/depression. The biological synaptic weight can be persistently changed by modulating the amount of neurotransmitter presynaptically released across the synapse or the number of receptors present postsynaptically; this is so-called long-term plasticity. Specifically, the increases and decreases in synaptic weight are called long-term potentiation (LTP) and long-term depression (LTD), respectively as shown in figure 7c [13]. After synaptic modulation, different types of memory behaviors form. Short-term memory (STM) involves temporary changes in synaptic strength, facilitating the transient storage of information, while long-term memory (LTM) relies on persistent modifications that enhance specific connections between neurons, enabling the storage and retrieval of memories [14]. It is necessary to create devices that can mimic the basic processes of biological synapses in order to produce neuromorphic systems. Our focus is to develop a cost-effective, stable and compatible three terminal artificial synaptic device based on ion movement.



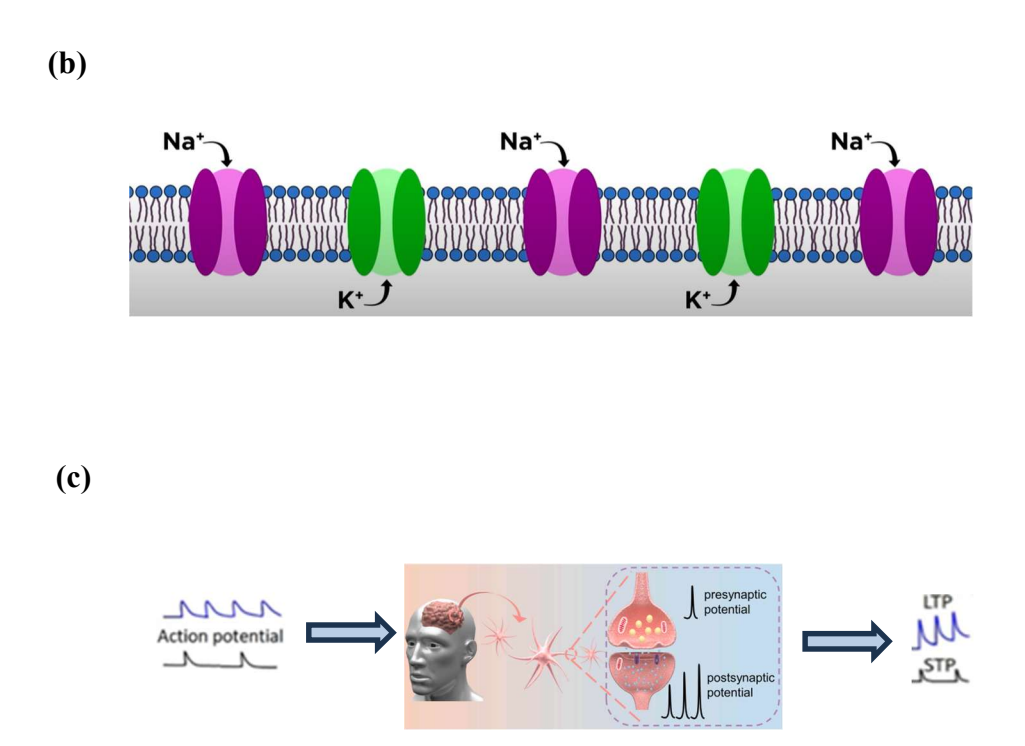


Figure 7: Biological neural systems. **(a)** Schematic structure of biological neural systems consisting neurons and synapses ^[15]. **(b)** signal transmission across the cell membrane ^[12]. **(c)** Synaptic properties, including various learning and forgetting functions ^[13].

1.5 Multi armed bandit problems (MBPs):

Multi-armed bandit problems have been an active area of research since the 1950s. The problem can be stated as follows (J.C. Gittins, 1979): there are N arms, each having an unknown success probability of emitting a unit reward [16]. The success probabilities of the arms are assumed to be independent of each other. The objective is to pull arms sequentially so as to maximize the total reward. Decision-maker device is frequently used in

the fields of computation and information technology to get better results in a broad range of current intelligence activities. The decision-maker device will be developed on the basis of ion movement. The decision-making device is able to solve different multi armed bandit problems (MBPs) [17]. In probability theory and machine learning, a decision maker must select among several options while only a portion of each option's characteristics are known. This is known as the multi-armed bandit (MAB) issue. The goal is to maximize the total rewards over time by finding the best action or the one with the highest chance of giving a reward as shown in fig-8 [18]. Our target is to develop synaptic based ionic decision-maker device which is used in communication network.

A - 1 \$\infty\$ Win: rewarded \(\bigcap_{A} \) SM A \(\text{SM B} \) select and play \(\text{SM A} \) SM B \(\text{SM B} \) Select and play \(\text{SM A} \) SM B \(\text{SM B} \) \(\text{SM Channel A} \) \(\text{Channel B} \) \(\text{Channel B} \) \(\text{Channel B} \)

Figure 8: (A) 1: Illustration of MBP. Gambler selects and plays slot machines to maximize total reward. 2: MBP in the channel model, in which a communication network user attempts to select an available channel ^[18].

1.6 Focus of the work:

1.6.1 The substrate:

Typically, insulating substrates are used to deposit WO₃ films. Here, Li-Ion Conducting Glass Ceramic (LICGC) has been selected as the substrate. Because it functions as a solid electrolyte, it can be utilized as a source of Li-ions to aid in the lithiation of WO₃. It has a low surface roughness assuring intimate contact with the film being deposited.

1.6.2 The electrode:

The structure of a gas sensor device and artificial synaptic based ionic decision maker device consists of the top electrode which is the sensing electrode and a bottom electrode. The choice of material is very crucial for the top electrode. We have chosen WO₃ as the sensing electrode in this work. As a typical N-type semiconductor, WO₃ with a wide bandgap of 2.6 eV has attracted considerable research attention because of its superior stability and high electron mobility and has been extensively applied in gas sensors ^[19]. The high surface reactivity of WO₃ makes it very effective in adsorption of gases, leading to significant changes in its electrical properties when exposed to different gases. WO₃ is chemically stable and mechanically robust, which makes it suitable for use in harsh environments. Its stability ensures that the sensor characteristics do not degrade significantly over time, which is important for long-term applications.

1.7 Methodology:

The device was made from thin films. The technology available for their manufacturing determines the creation of improved devices. Since it allows for the shrinking of current devices and improves cost-effectiveness, thin film technology is important in the field of solid-state ionics. Using this technology, functional structures are created by applying thin layers of materials onto a substrate. Thin film technology has various benefits when used with solid-state ionic devices like integrated circuits (ICs), transistors, and sensors.

1.7.1 Thin film fabrication methods:

Thin films are layers of material ranging from a few nanometers to several micrometers in thickness. They are crucial in electronics, sensors, photovoltaics, and solid-state devices. There are several techniques for thin film fabrication. Some of the techniques are discussed in below:

1. DC Magnetron Sputtering:

Direct current (DC) magnetron sputtering is a physical vapor deposition (PVD) technique used to create thin films by ejecting atoms from a solid target and depositing them onto a substrate. A DC voltage is applied between a cathode (target) and an anode in a vacuum chamber filled with inert gas (typically argon). The DC power ionizes argon gas, creating Ar⁺ ions. Ar⁺ ions bombard the target material, knocking off atoms (sputtering). These atoms travel and deposit as a thin film on the substrate.

2. RF Sputtering:

RF (Radio Frequency) sputtering is a physical vapor deposition (PVD) technique similar to DC sputtering, but it uses radio frequency power (typically 13.56 MHz) to sputter both conductive and insulating materials. An RF generator applies an alternating electric field between the target (cathode) and the grounded chamber. In a low-pressure argon plasma, electrons and ions are generated. Ar⁺ ions bombard the target material, dislodging atoms from its surface. These atoms travel to the substrate and form a thin film.

3. Pulsed Laser Deposition:

Pulsed Laser Deposition (PLD) is a thin film deposition technique that uses high-energy laser pulses to ablate material from a solid target and deposit it onto a substrate. It is especially effective for creating complex oxide films with high stoichiometric accuracy.

4. Doctor Blading:

Doctor blading, also known as tape casting, is a simple and costeffective thin film fabrication technique used for depositing uniform films, especially of ceramic or composite materials. A slurry mixture is made and cast onto one side of the substrate and then spread by a blade to obtain uniformity.

5. Spin Coating:

Spin coating is a widely used technique for depositing thin, uniform films on flat substrates. It's particularly popular for oxides, polymers, resists, and sol–gel-derived materials like WO₃, TiO₂, or perovskites. A small amount of liquid precursor (sol or solution) is dropped onto the center of a clean substrate. The substrate is rapidly spun at high speed (typically 1,000–8,000 rpm). Centrifugal force spreads the solution outward, while solvent evaporates simultaneously. This results in a thin, uniform film, typically in the range of 20 nm to a few microns, depending on parameters.

Our focus is only on direct current (DC) magnetron sputtering for thin film deposition on solid electrolyte.

Chapter 2: Literature Review

The industry for rechargeable batteries was entirely changed by the groundbreaking discovery of lithium-ion batteries. John B. Goodenough, M. Stanley Whittingham, and Akira Yoshino were awarded the 2019 Nobel Prize in Chemistry for the invention of lithium-ion battery. They also significantly contributed on technology ranging from electric vehicles to portable devices. The lithium-ion battery was first created in the 1980s. Using liquid electrolytes in early designs raised serious concerns due to the potential for flammability and safety problems. As a result, scientists looked into safer options, and solid electrolytes showed promise. All solid-state lithium-ion batteries have become the new ideal candidate for energy storage. The shift to solid electrolytes has inspired the development of new kinds of solid-state devices. It suggests that the design principles of solidstate batteries could be extended to create a variety of functional devices beyond batteries. These new devices could find applications in gas sensing, decision-making systems, artificial neuromorphic system, and even AIdriven technologies. This motivated us further to explore the use of using battery materials for solid-state ionic devices. The first device is a gas sensor device that aims to sense ethylene, an essential gas in the agricultural industry. Food spoilage can be prevented by timely detection of ethylene, as fruits and vegetables produce this gas on ripening. This will help reduce the wastage of agricultural produce. The device structure is straightforward, consists of a sensing electrode, a solid electrolyte, and a counter electrode.

The material of choice for the sensing electrode is WO₃, a semiconductor widely used in gas sensing. The second device, the artificial synaptic based ionic decision maker device, is important for solving different DMBPs, which are normally difficult task to predict the correct result due to the Nash

Equilibrium [20]. A multi-armed bandit problem is a reinforcement learning challenge where a decision-maker (the bandit) must select the best action from multiple options (arms) to maximize a reward over time. Each arm has an unknown reward distribution, and the objective is to identify the most rewarding arm. Balancing exploration (trying various arms to learn their rewards) and exploitation (choosing the arm with the highest estimated reward) is a critical aspect of this problem. The ionic decision-maker device which is mentioned in this report will be developed on the basis of solid state ionics. Ionic decision-maker device can also be used to predict the human behaviours, from microscopic system to macroscopic system. The ionic decision-maker devices are also able to predict the artificial synaptic plasticity (LTP and STP) behaviour in human neurons. From the data, we can be easily predicted the complex personality for a single synapse of human neurons [21]. The LICGC is used in ionic decision maker as a solid electrolyte [22]. By changing Li ion concentration, the decision maker device will be developed.

It excites me to investigate Li-ion ceramic conductors and their potential beyond conventional energy storage, especially in light of their thin-film applications. These ceramics are commonly found in the market as millimeter-sized pellets. It is demonstrated by their capacity to decrease size and increase performance in devices like chemo-resistive gas sensors. Their integration into fields like neuromorphic computing, artificial intelligence, and gas sensing presents a promising future for solid-state devices. The evolution of devices is highly dependent on the performance of their computational units. Traditionally, these are made of silicon, which was widely used during the industrial revolution. Li-ion ceramics have proven to be a good candidate to substitute silicon in some, if not all, devices, also imparting superior device performance. Their integration into gas sensing devices has enabled highly selective and sub-ppm level sensing performance. Gas sensor devices work on the basis of the change of resistance on the adsorption of gas on the surface of metal oxide [23].

A sensor is a device that transforms a physical quantity into a signal that can be interpreted by a person or an electronic device. It is often referred to as a detector or a transducer. A gas sensor is a type of transducer that identifies gas molecules and generates an electrical signal whose intensity correlates with the gas concentration. The detection of gases primarily involves chemical processes, whereas the conversion of this detection into a signal involves physical processes. This implies that the detection is highly influenced by external conditions, particularly temperature.

The sensitivity of the sensor response depends greatly on both the type of receptor employed and the temperature at which it operates. There are many types of gas sensors based on working principles and structure. Out of these, the chemiresistive gas sensors widely employ metal oxide semiconductors for the sensing layer. Chemiresistive gas sensors function based on the principle of changes in electrical resistance that occur when the semiconductor material interacts with gases.

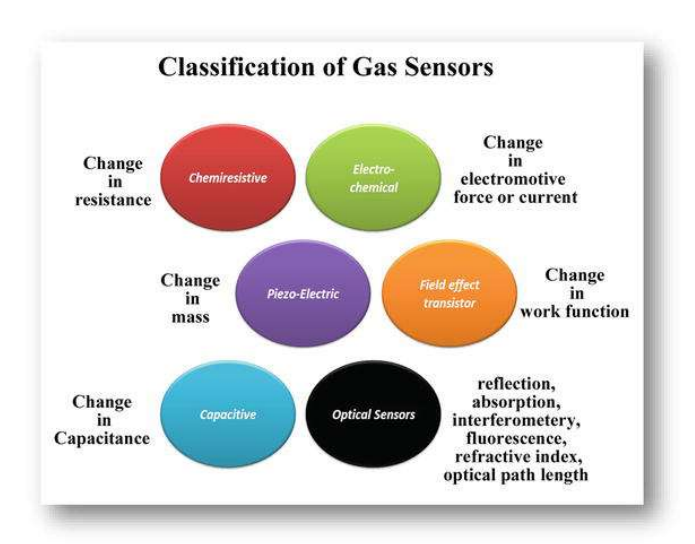


Figure 9: Different types of gas sensor device.

Using thin films for sensing can help develop cost-effective, efficient and fast-response devices. The gas sensors comprise of the sensing electrode and counter electrode on either side of the solid electrolyte. Semiconducting materials are generally reported to have good sensing ability as their interaction with the gas can tune the band gap that also reflects in their electrical properties. The target gas here is ethylene, an important gas in the agriculture industry. ZnO and SnO2-based sensors have been reported previously [24][25][26]. But the high operating temperatures of 350-450 °C do not make them very suitable for direct use. Their application in real-time is limited by their poor stability, low cyclability, and high operating temperatures. Overcoming these hurdles can ensure the use of gas sensors at the industrial level. LICGC is used as the solid electrolyte in both devices. LiCoO₂ is a cathode material with layered oxide structure which was first reported by John B. Goodenough [27]. LiCoO₂ was used first as a cathode material in Li ion battery. It is now the most commonly used cathode material. Their integration into other functional devices has been studied extensively. However, there are very few reports on their use in gas sensing devices. Ethylene gas sensing has been reported by various groups using SnO₂ and ZnO as the sensing electrode ^{[28][29]}.

Here, the focus will be on the impact of doping on its characteristic properties of WO₃ on the gas-sensing. The synthesis of all-solid-state devices can be challenging when it comes to scaling down the size to the micron level. Good device capacity is to be maintained while electrode volume will also be low. Thin films are the solution to satisfy all requirements. Various types of techniques such as pulsed laser deposition [30], DC magnetron sputtering, spin coating, doctor blading etc. for thin film deposition. Each of these techniques has a specific maximum value for film thickness and is chosen accordingly to suit the needs. In case of PLD, the laser beam is incident on the target which has enough energy to create a

plasma plume by ejecting out the material. This plasma plume drifts towards the substrate and deposits a layer onto it. Spin coating [31] and doctor blading [32] are comparatively easier techniques that involve the use of liquids. In spin coating, the required material is prepared by the sol-gel method and coated onto the substrate multiple times with intermittent heating to obtain the required thickness. In doctor blading, a slurry is prepared which is drop cast on the surface and spread evenly using a glass slide to get a homogeneous layer.

An artificial neuromorphic system, synaptic devices mimic biological synapses in terms of multi-state memory, in-memory computing, and nonvolatility properties [33]. In 2008, Hewlett-Packard Company presented titanium dioxide thin film with adjustable resistance and time-dependent memory characteristics. It is believed to be the first synaptic device realized through a single electronic component [34]. Since then, growing efforts have been made to fabricate synaptic devices with diverse structures and working mechanisms. Nowadays, artificial synapses are mainly classified into two types according to their device structures: two terminal memristors and three-terminal synaptic transistors. Taking inspiration from the three terminal devices, our goal is to prepare three terminal artificial synaptic modulated gas sensing devices. Recently, biomimetic sensory systems based on the incorporation of advanced sensing technologies and synaptic devices have also become hot issues. By mimicking the neurobiological architecture of biological sensory organs, they provide a neuromorphic way to perceive, transmit, and process sensory information, which helps promoting a notable evolution in next-generation humanoid robotics, prosthetics, wearable electronics, and etc. Figure 10 shows the frame work of the advantages of synaptic devices and their applications in biomimetic sensory neural systems [35].

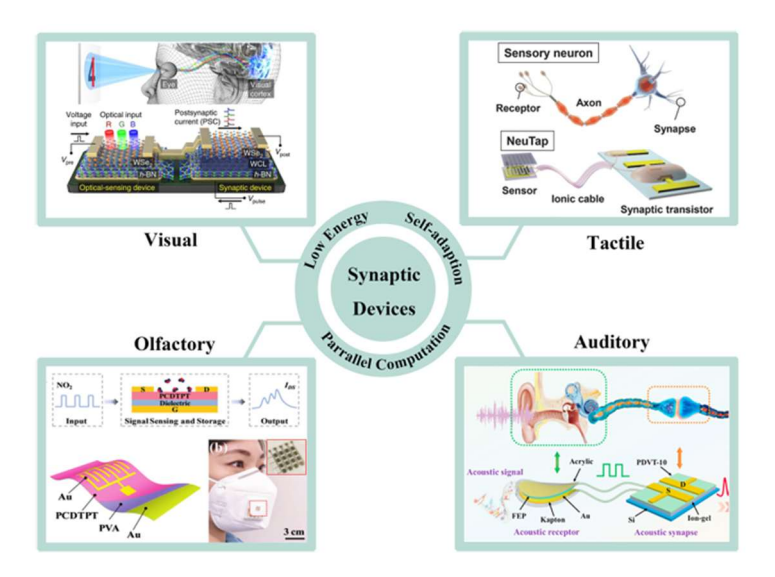


Figure 10: Advantages of synaptic devices and their applications in biomimetic sensory neural systems ^[35].

Chapter 3: Objectives

1. The first objective of my project is the development of solid-state lithionics based on room temperature ethylene gas sensing for detecting fruit ripening and fruit spoilage in storehouses.

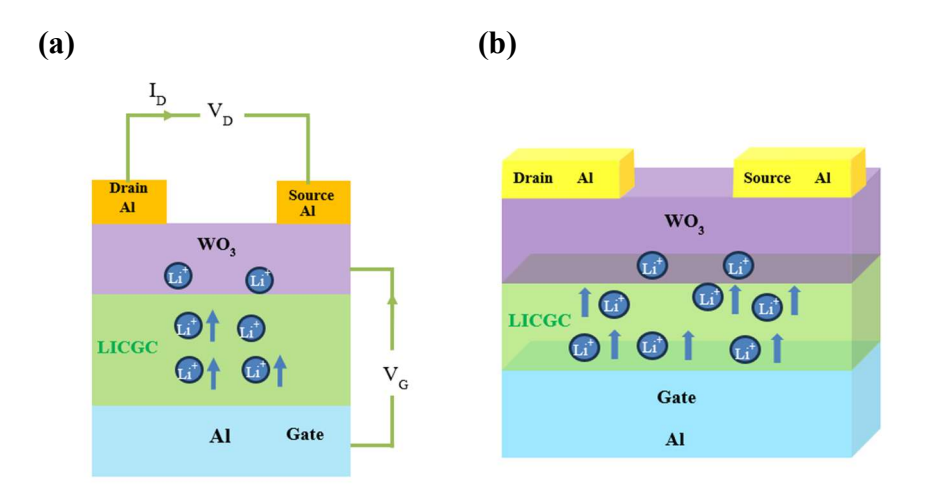


Figure 11: (a) Schematic diagram of gas sensing device. (b) top view of gas sensing device.

2. The second objective of my project is the development of a solidstate lithionics based artificial synaptic ionic decision maker device to solve different multi armed bandit problems and mimic the biological synaptic behaviour like short term and long-term potentiation.

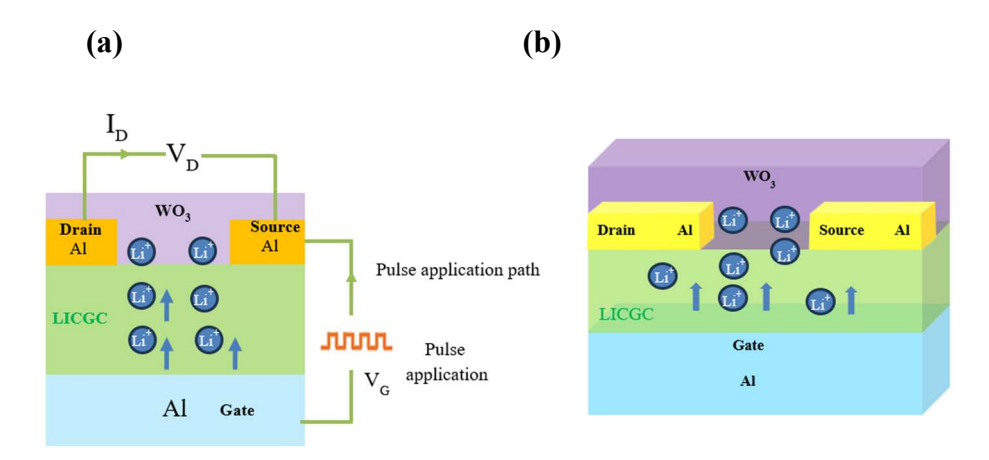


Figure 12: (a) Schematic diagram of artificial synaptic ionic decision-maker device (b) top view of artificial synaptic ionic decision-maker device.

Chapter 4: Experimental Section

4.1 Materials used:

Al-doped LLZO powder was purchased from Sigma Aldrich (≥99.5% purity). The composition of LLZO powder is Li_{6.24}La₃Zr₂Al_{0.24}O_{11.98}. Tungsten metal of 99.5% purity was purchased from TCI. PVA (polyvinyl alcohol) of molecular weight ~30,000 from TCI was used. Aluminum and titanium metal was also purchased from TCI. Al and Ti were used for the gate, drain and source electrode of the device. The final device was fabricated using LICGC having composition Li₂O-Al₂O₃-SiO₂-P₂O₅-TiO₂-GeO₂. LICGC was purchased from Ohara corporation. The LICGC is a glass ceramic having high ionic conductivity of up to 10⁻⁴ S cm at room temperature (comparable to liquid electrolytes) [^{36]}. LICGC has a low roughness surface. Due to low surface roughness of LICGC which allows for the formation of good contact with the film. Annealing was done in a tube furnace and muffle furnace.

4.2 Chemicals required:

- Polyvinyl Alcohol
- Ethanol
- Acetone
- Isopropyl Alcohol

4.3 Device fabrication and experimental set up:

4.3.1 LLZO pellet formation for substrate electrode:

2 gm LLZO powder was taken in a mortar pestle. Then, 2% polyvinyl alcohol solution was added to the powder and grinded the LLZO powder properly for 2 minutes. Here, PVA solution acts as a binder. Acetone was added to the powder and grinded the powder for 5 minutes. After proper

grinding, the powder was dried by IR-lamp for 10 minutes. Again, acetone was added to the dried powder and grinded the powder for 5 minutes. The powder was dried by IR-lamp for 10 minutes. Then, 15 mm SS pellet die was filled by the dried Al-doped LLZO powder. The pellet was formed by the hydraulic press. 5 tons pressure was applied for 5 minutes to form the pellet by the hydraulic press.

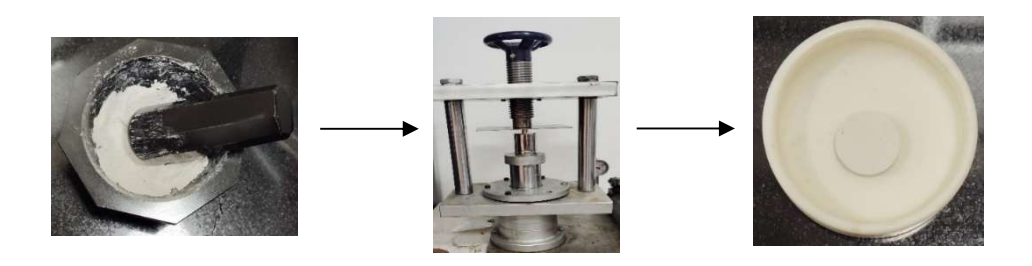


Figure 13: Schematics diagram Al-doped LLZO pellet formation.

4.3.2 Conventional sintering of the LLZO pellet:

The LLZO pellet was placed in muffle furnace by the alumina crucible. The pellet was sintered at 1050 °C for 12 hours to increase the density of the LLZO pellet by the muffle furnace. The dense LLZO pellet is required as solid electrolyte for preparing gas sensor device. Unfortunately, the pellet was obtained by this method was unsuitable due to the density of the sintered pellet was not high enough for handling, cutting and polishing. The sintered pellet was characterized by XRD.

4.3.3 Dense Al-doped LLZO pellet formation by SPS:

2 gm sintered (800 °C for 2 hr) Al-doped LLZO powder was taken in 20 mm graphite die. The graphite die was placed inside the spark plasma sintering chamber. The target temperature for the pellet formation was 800 °C. The target temperature was applied for 5 minutes. The pressure was applied for the pellet formation. The amount of applied pressure was 12 kN. The pressure was applied for 5 minutes. The heating rate was 50 °C/min. The instrumentation set up of spark plasma sintering is shown in figure 14. But the pellet was obtained by this method was also unsuitable as solid electrolyte for preparing synaptic and gas sensor device. The sintered pellet was characterized by XRD.

SPS is a pressure-assisted pulsed current sintering, in which densification is favoured over coarsening and occurs at lower temperatures than in the conventional process. The SPS process usually combines very efficient densification with a fine control of grain structure. The applied pressure may induce texture in the case of anisotropic grain shape in to-be-densified powder [37, 38]. In the SPS experiments, the metal oxide powders are loaded into a graphite die lined with graphite paper to prevent contamination of the die.

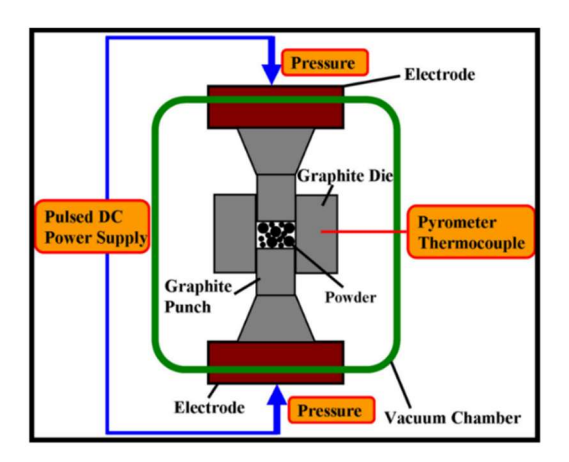
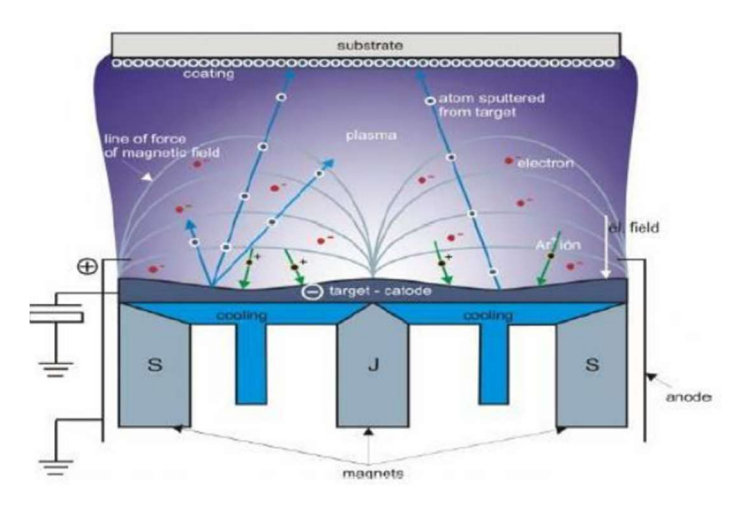


Figure 14: Schematic diagram of a Spark Plasma Sintering equipment.

4.3.4 Deposition of tungsten oxide (WO₃) on LICGC substrate:

Tungsten oxide thin film was prepared by DC magnetron sputtering and annealed in Ar atmosphere. The target was W metal disc (purity 99.95%), which was 2" mm in diameter and 3 mm in thickness. The LICGC substrate length was 10×10 mm. Magnetron sputtering was done in a mixed atmosphere of sputtering Ar gas (15 sccm) and reactive O_2 gas (8 sccm). The deposition was performed at room temperature [39]. The thin film sample was prepared by the deposition of WO₃ followed by annealing for 1



hr at 450 °C. The instrumentation set up of DC magnetron sputtering is shown in figure 15.

Figure 15: Schematic layout of a typical DC magnetron sputtering unit.

4.3.5 Deposition of Al metal on sputtered WO₃ thin film and LICGC substrate:

The bottom side of the device and the top side of the deposited WO₃ thin film for source and drain electrode was deposited with aluminum metal by DC magnetron sputtering on LICGC substrate. The target was Al metal disc (purity 99.99%), which was 3" mm in diameter and 3 mm in thickness. Magnetron sputtering was done in inert atmosphere of sputtering Ar gas (10 sccm). The deposition was performed at room temperature. The deposition was done for 30 minutes. The final device Al/LICGC/WO₃/Al and Al/LICGC/Al/WO₃ was analyzed by SEM, XRD, AFM and Raman spectroscopy and then used for gas sensing study and artificial synaptic study.

4.3.6 Artificial synaptic device I-V characteristic studies:

The synaptic characteristics of the device was checked by Keithley instrument. In Keithley instrument, we can measure the relation between voltage and current with time. In Keithley, I used two channels for checking the I-V characteristics of the device. In red wire of channel-1 of the Keithley was connected to the drain terminal of the device by probe manipulator and green wire of channel-1 of the Keithley was connected to the source terminal of the device by probe manipulator. Similarly, in red wire of channel-2 of the Keithley was connected to the gate terminal of the device and green wire of channel-2 of the Keithley was connected to the source terminal of the device. Here, the source acts as a grounding terminal. The circuit was prepared by bread board. I measured drain current (I_D) vs time, gate current (I_G) vs gate voltage (V_G), drain current (I_D) vs gate voltage (V_G) and also gate current vs time. The effect in situ doping of Li⁺ ion on thin film WO₃ was checked by Keithley instrument. The experimental set up is shown in figure 16.

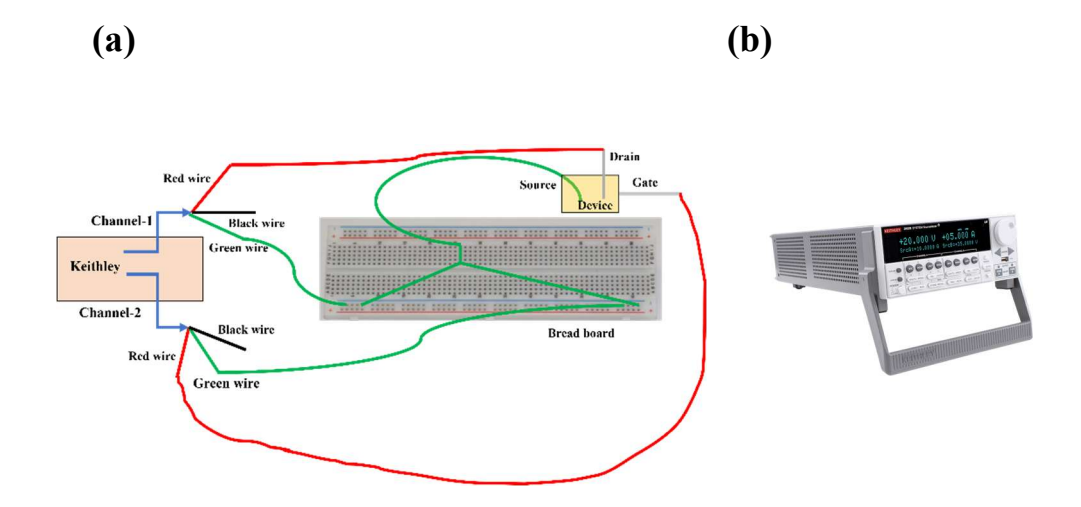


Figure 16: (a) The experimental circuit set up for the I-V measurement of synaptic device. **(b)** Picture of the Keithley instrument.

4.3.7 Gas sensing studies:

As shown in Figure 17, a gas sensing circuit connection was used to perform the gas sensing measurements. The sensor's operating temperature was controlled by a temperature controller. Silver paint and platinum wire were used to create electrical connections for charge transmission. Following that, the sensor was placed within a 10 L glass chamber. Using a syringe, gas was injected into the chamber to conduct the gas sensor investigations.

The voltage and temperature controller apparatus were connected to the Keithley instrument. The current was measured by the Keithley instrument at different room temperature.

Gas concentration was pre-determined using the formula:

Gas conc. (ppm) =
$$\frac{\text{Known injected vol of gas}}{\text{Vol of the chamber}} \times 1000$$

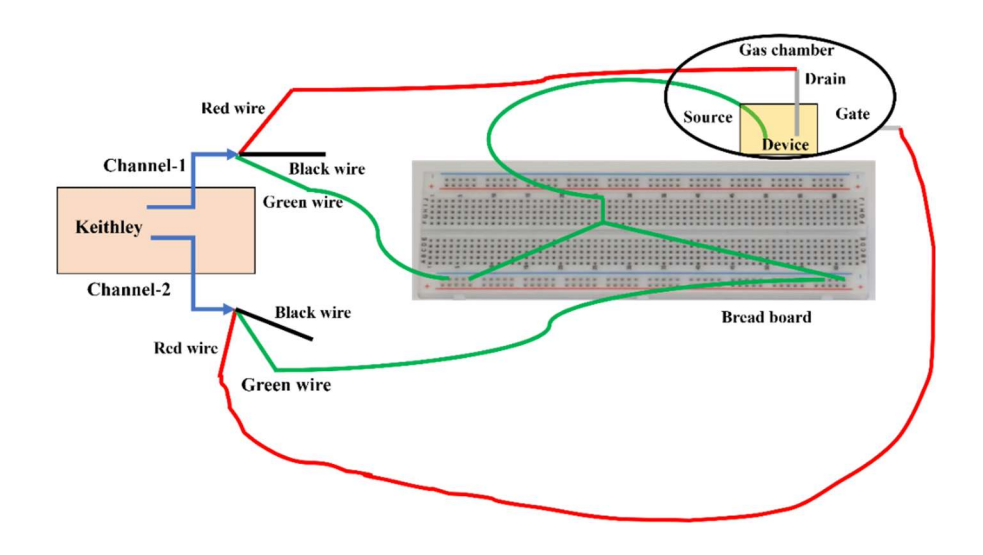


Figure 17: Gas sensing circuit set up

4.3.8 Instrumentation:

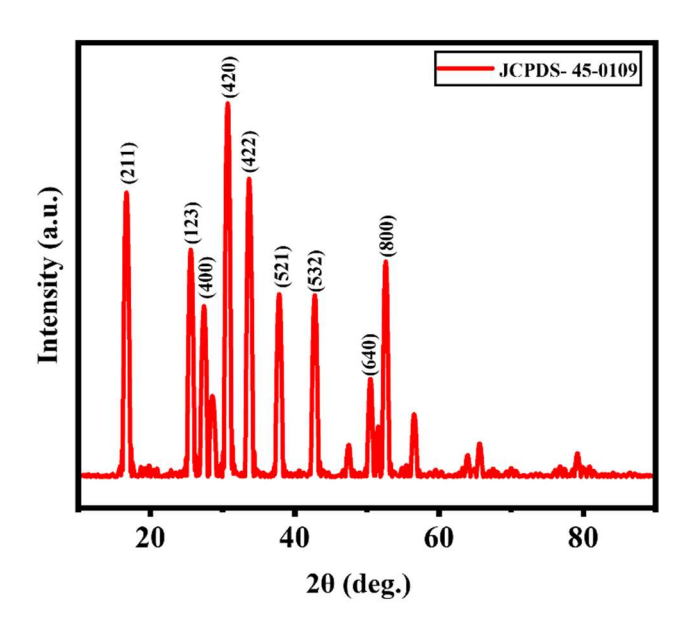
AFM studies were done using Park Systems NX10 Atomic Force Microscopy in non-contact mode (NCM). Supra 55 Zeiss field-emission scanning electron microscope was used to capture the FESEM images. X-Ray Diffraction spectra was analysed by XPert Highscore. Raman studies were carried out using LabRAM HR Evolution Raman Spectrometer. Electrochemical measurements were performed using Biologic 150. The TGA data was analysed by origin 2024b software. The I-V data was obtained by the Keithley 2604B instrument. The Keithley data was measured by kickstart software and the data was analysed by origin 2024b software. For the calculation of carrier concentration of the device, the hall instrument was used. The hall probe data was also analysed by origin 2024b software.

Chapter 5: Results and Discussion

First, the characterization of Al-doped LLZO powder and sintered LLZO powder have been discussed. Then the characterization of formed LLZO pellet by spark plasma sintering have been discussed. The synaptic device along with the gas sensing properties before and after lithiation have been discussed. The characterization of the final device has been explained. The mechanism of sensing has been discussed based on carrier concentration of WO₃ thin film. For checking the synaptic behaviour, I-V characteristics of the device have been performed using a Keithley 2604B Source Measure unit.

5.1 Characterization of LLZO powder and sintered LLZO powder:

(a)



(b)

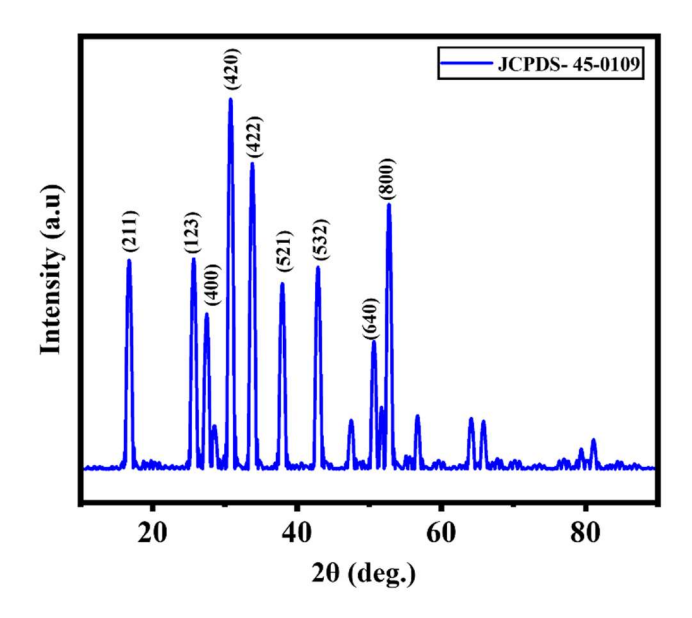


Figure 18: XRD data of **(a)** pure Al-doped LLZO powder (b) sintered LLZO powder.

The XRD of pure LLZO powder is shown in figure 18. The XRD data is matched with the JCPDS number- 45-0109 which corresponds to the cubic phase of Al-doped LLZO powder. The sintering was done for the Al-doped LLZO powder. The sintering was done at 800 °C for 2 hr by the muffle furnace. After sintering the XRD data of the powder was also taken for the confirmation of the phase loss.

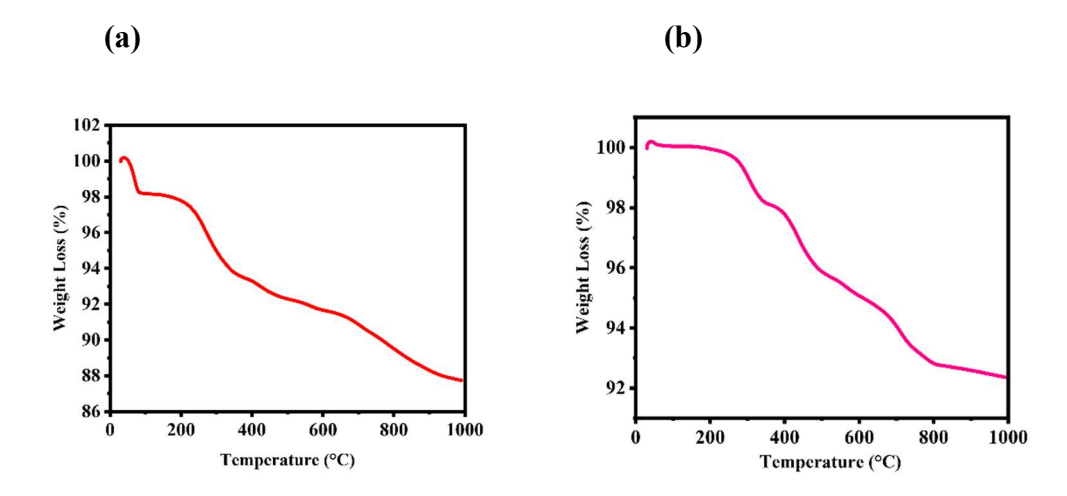


Figure 19: (a) TGA data of pure Al-doped LLZO powder **(b)** TGA data of sintered Al-doped LLZO powder.

TGA curve of Al-doped LLZO powder is shown in figure 19, heated to 0–1000 °C in an N₂-conditioned environment. Under 450 °C and between 550-850 °C, there were two distinct phases of significant weight loss ^[40]. The decomposition of La(OH)₃ was responsible for the 7.51% weight loss below 450 °C, whereas the creation of tetragonal and cubic LLZO was responsible for the 5% weight loss between 550 and 850 °C. The weight loss remained constant after around 950 °C, indicating that the full decomposition of the La(OH)₃. TGA data of sintered Al-doped LLZO powder was also recorded. There was no significant weight loss observed in TGA data. From the TGA data we concluded that Al-doped LLZO powder is stable at higher temperature also due to no significant phase loss at higher temperature for sintering.

5.2 Ethylene gas sensing study of the device:

5.2.1 In the pristine state:

The device was connected to the gas sensor and a constant voltage bias of 0.5 V was applied by the Keithley instrument to note the changes in the value of current upon insertion of gas into the chamber. The gas sensing study was done at different operating temperatures and different concentrations.

Figure 20 shows the gas sensing curves recorded at an operating temperature of 50 °C for 2 and 3 ppm of ethylene gas. Sensor response was recorded for the fruit to monitor the fruit volatiles production during ripening. Sensor response is calculated by the following SR (%) = $\frac{I_{gas} - I_{air}}{I_{air}} \times 100$ formula:

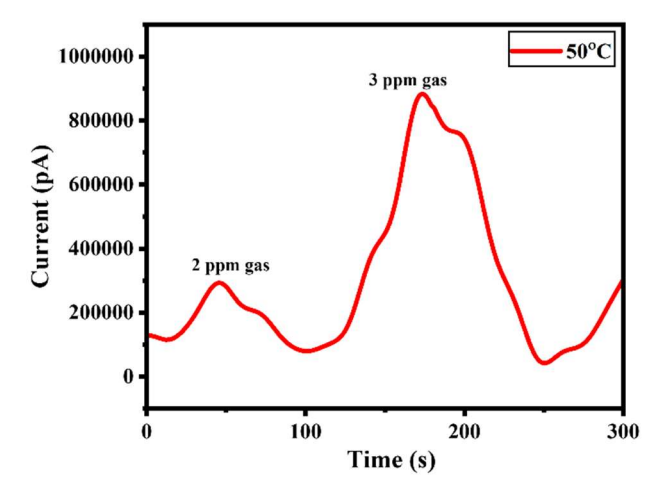


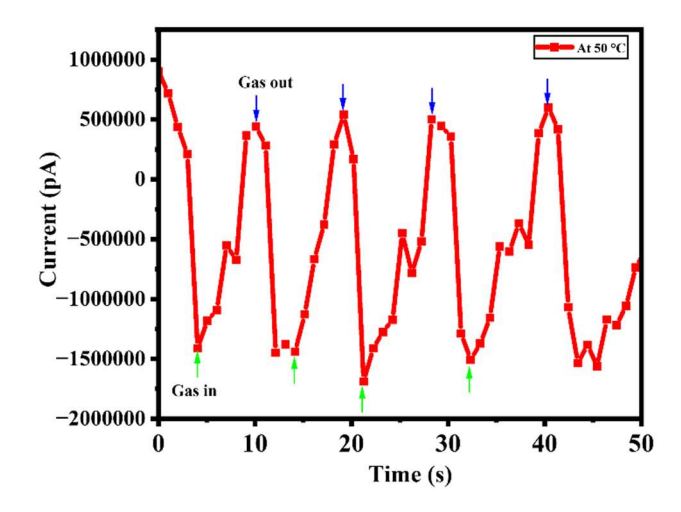
Figure 20: Ethylene gas sensing curves for 2 and 3 ppm of gas at an operating temperature of 50 °C.

A very high sensor response of 139 % and 675 % for 2ppm and 3 ppm of ethylene respectively was observed. The variation of sensor response to a fixed concentration of gas was measured. The film fabrication technique is very facile and yet has a very high sensitivity.

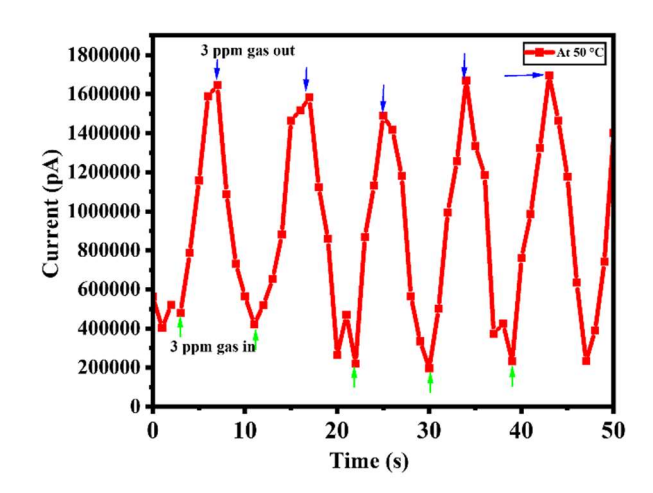
5.2.2 In the lithiated state:

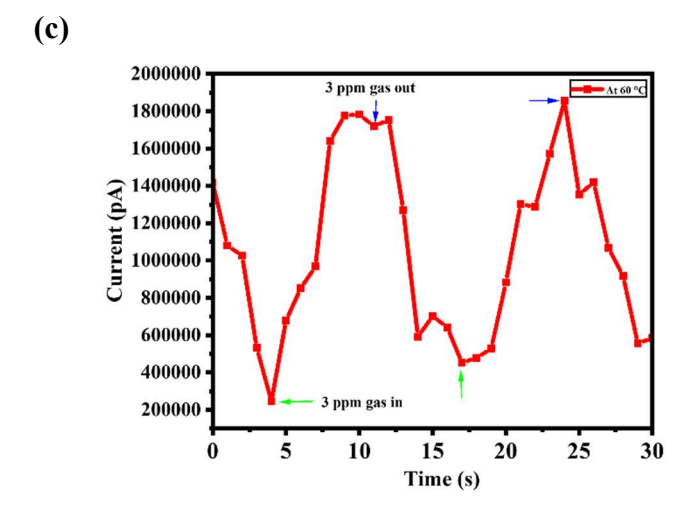
The gas sensing device was connected to the gas sensor and different constant bias voltage was applied by the Keithley instrument to note the changes in the value of current upon insertion of gas into the chamber. The gas sensing study was done at different operating temperatures and 3 ppm concentration.

(a)



(b)





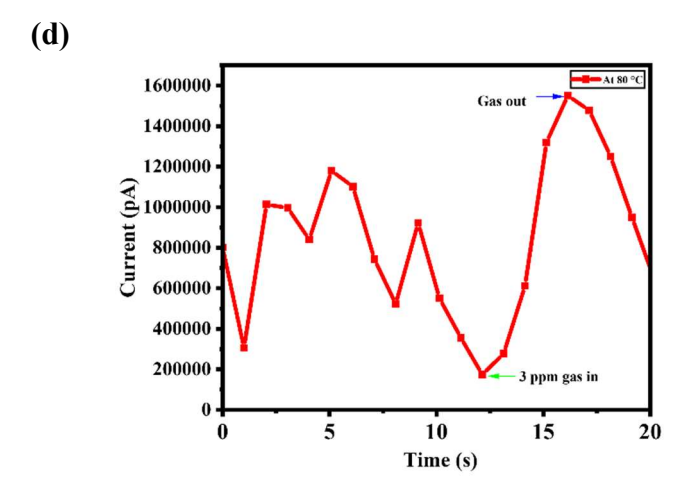
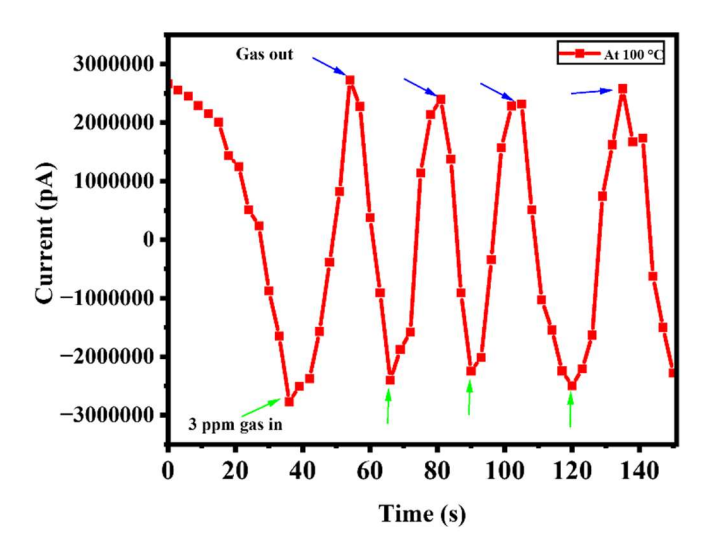


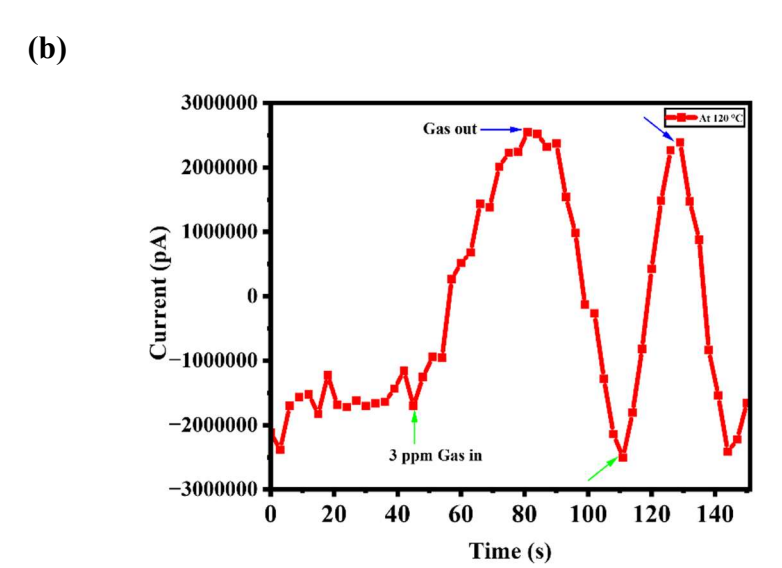
Figure 21: Ethylene gas sensing curves for 3 ppm of gas (a) at an operating temperature of 50 °C and constant bias voltage -5 V (b) at an operating temperature of 50 °C and constant bias voltage 5 V (c) at an operating temperature of 60 °C and constant bias voltage 7 V (d) at an operating temperature of 80 °C and constant bias voltage 5 V.

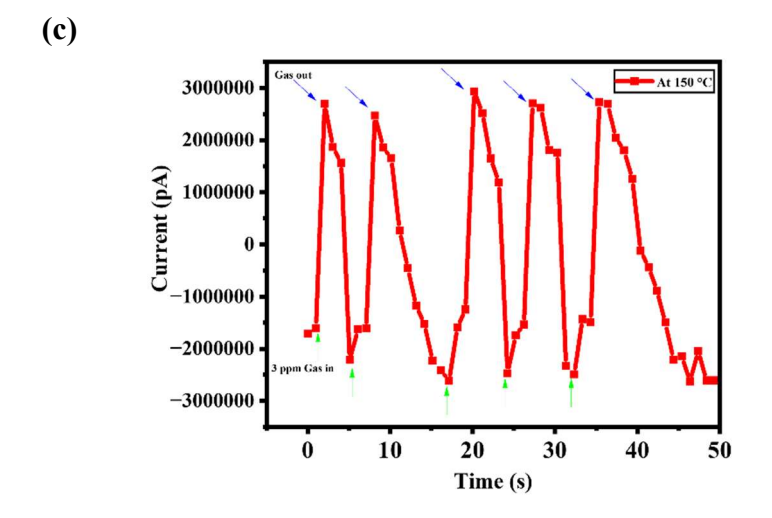
In all of the above cases the sensor response of the gas sensor device was significantly increases. The sensor responses were 133.33 %, 240%, 500% and 650% respectively. Such high values of sensor response for ethylene have never been recorded.

The gas sensing study was also done at different high operating temperatures and 3 ppm concentration. The gas sensing instrument was connected to the keithley source measure unit to observe variation of the current after the ethylene gas passing. The experiment was done at constant bias voltage at dc mode.

(a)







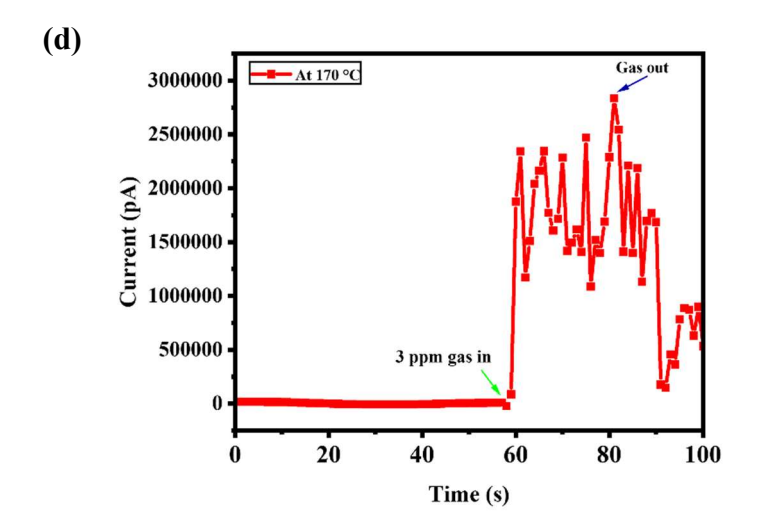
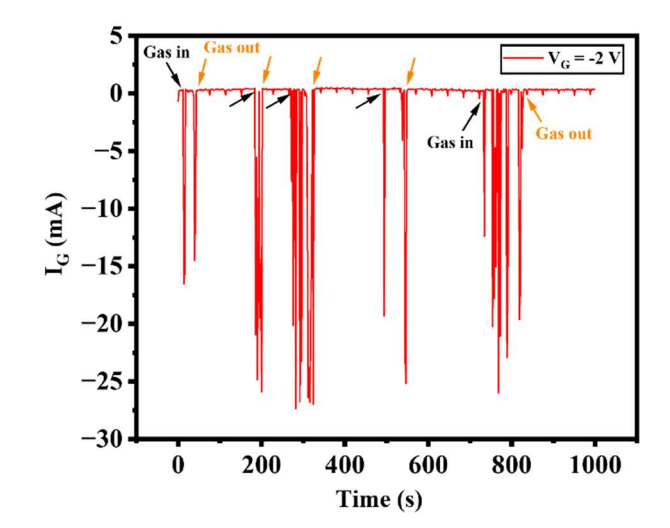


Figure 22: Ethylene gas sensing curves for 3 ppm of gas **(a)** at an operating temperature of 100 °C and constant bias voltage 10 V **(b)** at an operating temperature of 120 °C and constant bias voltage 10 V **(c)** at an operating temperature of 150 °C and constant bias voltage 5 V **(d)** at an operating temperature of 170 °C and constant bias voltage 5 V.

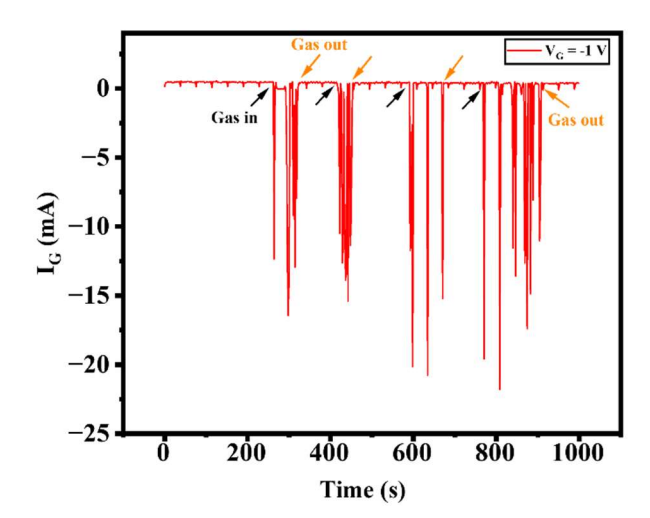
At higher temperature the device was responded very significantly. The sensor responses were 213.04 %, 203.70%, 293.33% and 2700% respectively. The gas sensor device was responded very significant sensor response at 170 °C. From there we concluded that the device was very effective at higher temperature.

The gas sensing device was connected to the gas sensor and different constant bias voltage was applied by the Keithley instrument to note the changes in the value of current upon insertion of gas into the chamber. The gas sensing study was done at room temperature and 3 ppm and 5 ppm concentration of ethylene gas. This experiment was done for pulse mode. For the experiment the three terminal of gas sensing device were used. The gas sensing instrument was connected to the keithley source measure unit. The drain terminal of the device was connected to the positive terminal of channel-1 of keithley instrument and source terminal was connected to the negative terminal of the device was connected to the negative terminal of channel-2 of keithley instrument and source terminal was connected to the negative terminal of channel-2 of keithley instrument. The experiment was done at constant drain voltage 0.5 V.

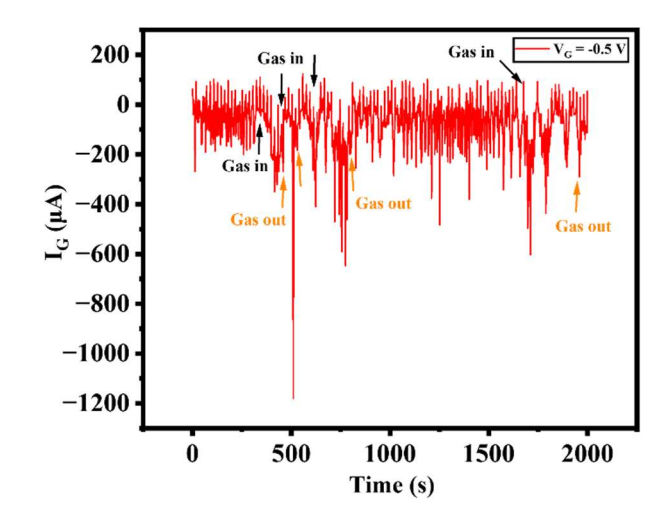
(a)



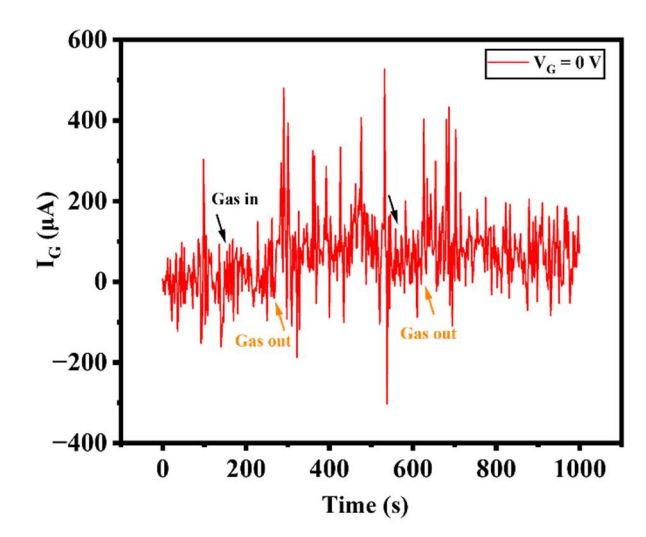
(b)



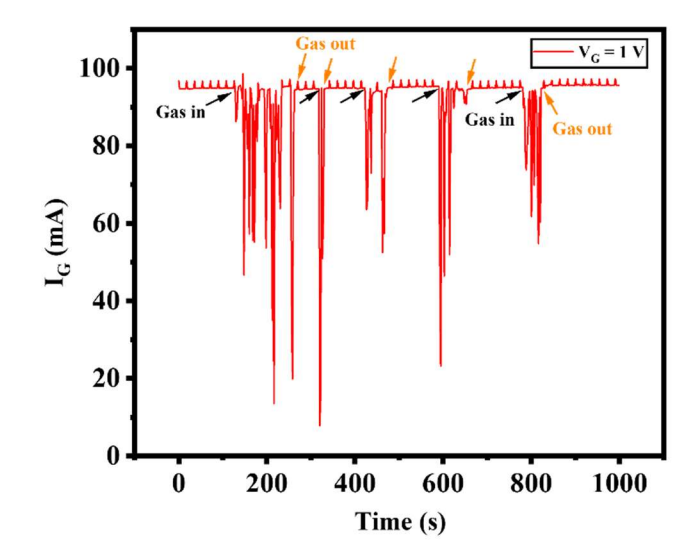
(c)



(d)



(d)



(e)

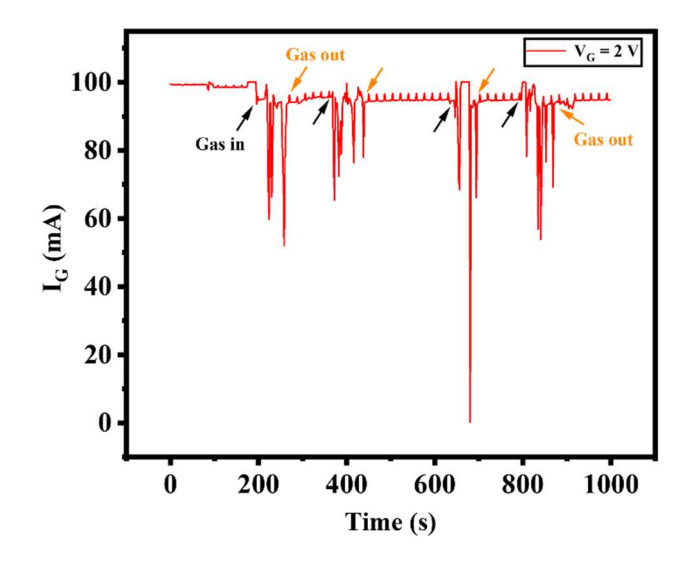


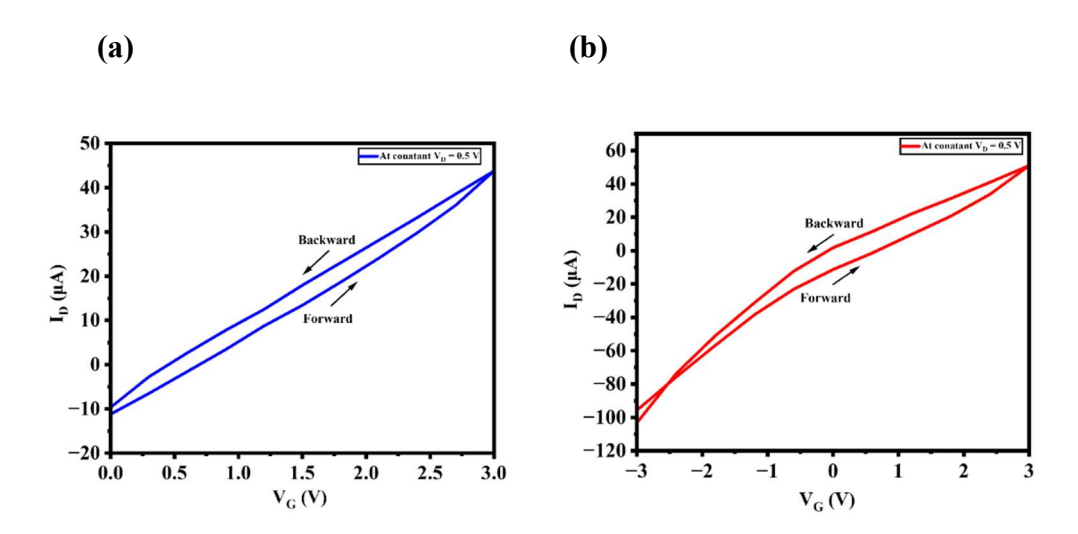
Figure 23: Ethylene gas sensing curves for 3 ppm and 5 ppm of gas at room temperature of 25 °C and (a) constant gate voltage -2 V (b) constant gate voltage -1 V (c) constant gate voltage -0.5 V (d) constant gate voltage 0 V.

(e) constant gate voltage 1 V (f) constant gate voltage 2 V at constant drain voltage 0.5 V.

All of the cases the current was decreases after the gas passing. This means that the resistance of the device was increases at above particular condition. This happens due to the decrease of major carrier concentration of the device. After gas passing the hole concentration of the device was increases and hence the major carrier concentration electrons were decreases. Due to decrement of major carrier concentration, the current was decreased.

5.3 Synaptic behaviours study of the device:

The synaptic study of the device was done by the keithley source measure unit. The experiment was done at dc mode. The circuit was made for the experiment by bread board. The three terminal of the device was connected to the keithley instrument by the bread board. The experiment was done at constant drain voltage 0.5 V.



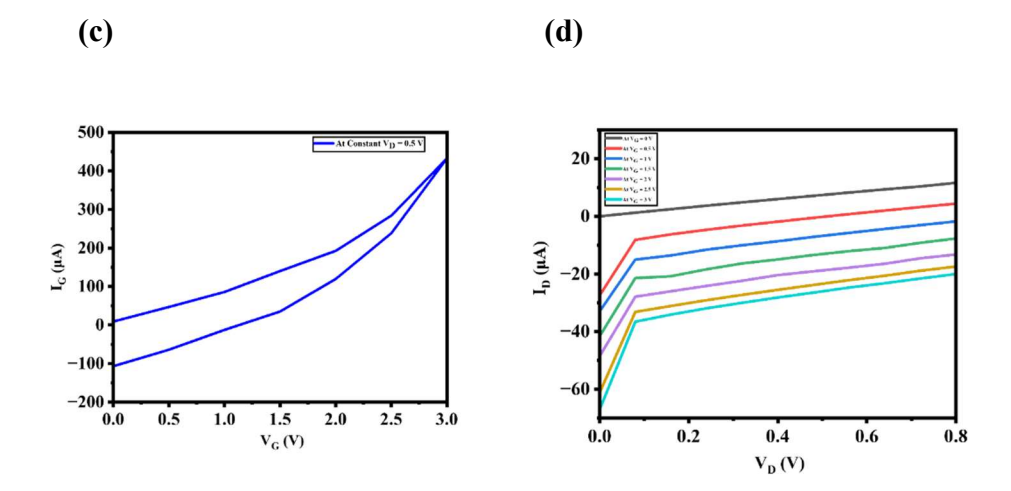


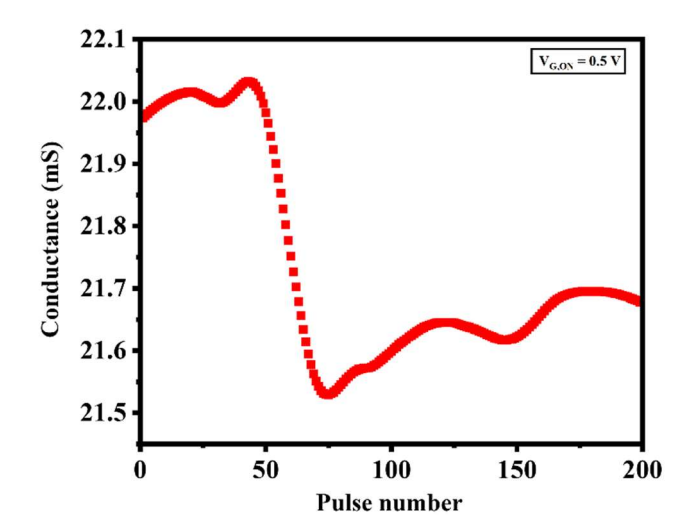
Figure 24: (a) and (b) Drain current change during V_G sweep of the device at constant $V_D = 0.5 \ V$ (c) Gate current change during V_G sweep of the device (d) Drain current change during V_D sweep of the device at different V_G .

Due to deposition of WO₃ on the LICGC substrate, depletion region was formed. When Li⁺ ion was entered into the WO₃ thin film, current was increased significantly due to the electrochemical reduction of oxygen atom. When gate voltage was decreased, the drain current and gate current was also decreased due to the sluggish kinetics of Li⁺ ion removal. But, increasing gate voltage the drain current of the device was decreases. This was happened due to increase of minor carrier concentration of the device. The holes concentration increases and the electron concentration decreases. Due to decrement of electrons concentration, the drain current was also decreased.

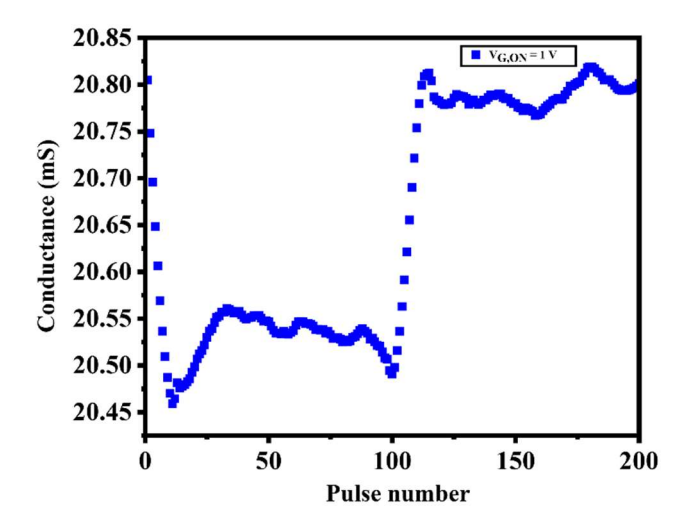
The synaptic study of the device was done by the keithley source measure unit. The experiment was done at pulse mode. The circuit was made for the experiment by bread board. The three terminal of the device was connected to the keithley instrument by the bread board. The experiment was done at constant drain voltage 0.5 V. The experiment was carried out at different

gate on voltage, different gate off voltage, different frequency and different amplitude.

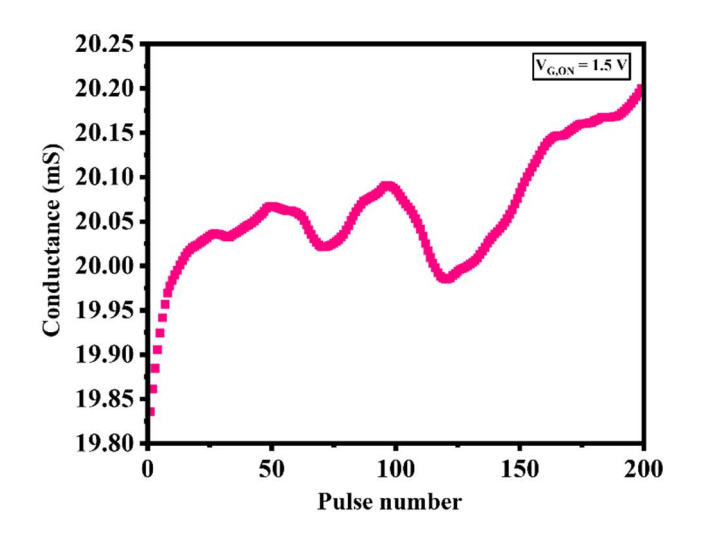
(a)



(b)



(c)



(d)

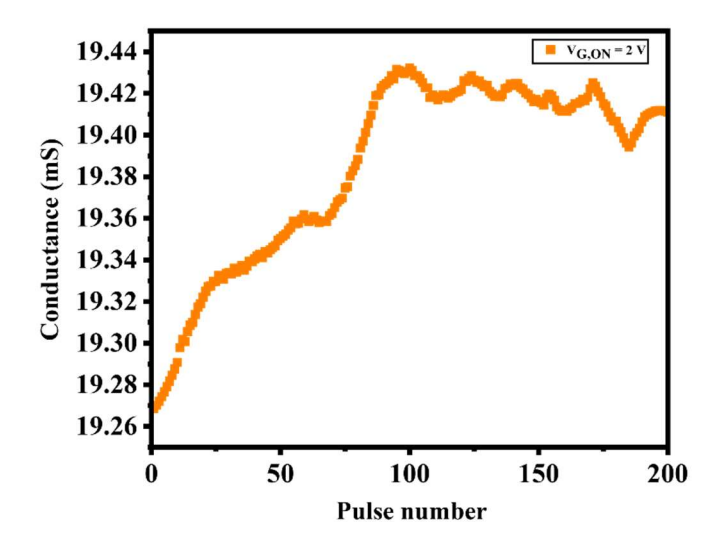
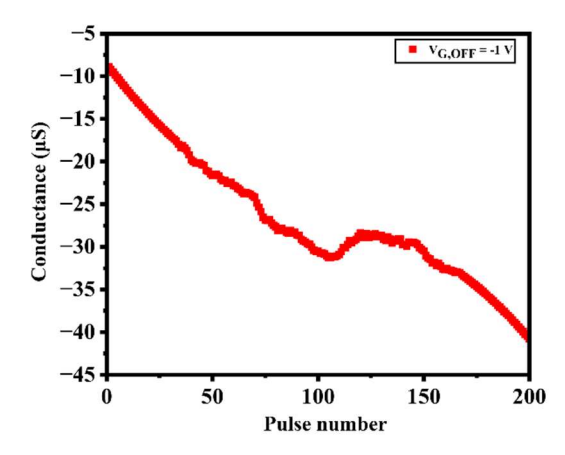


Figure 25: Potentiation–depression curves of synaptic device at constant drain voltage $(V_D) = 0.5 \text{ V}$ and at same off gate voltage $(V_{G, OFF}) = 0.3 \text{ V}$, at $V_{G, ON}$ voltage (a) 0.5 V (b) 1 V (c) 1.5 V (d) 2 V respectively.

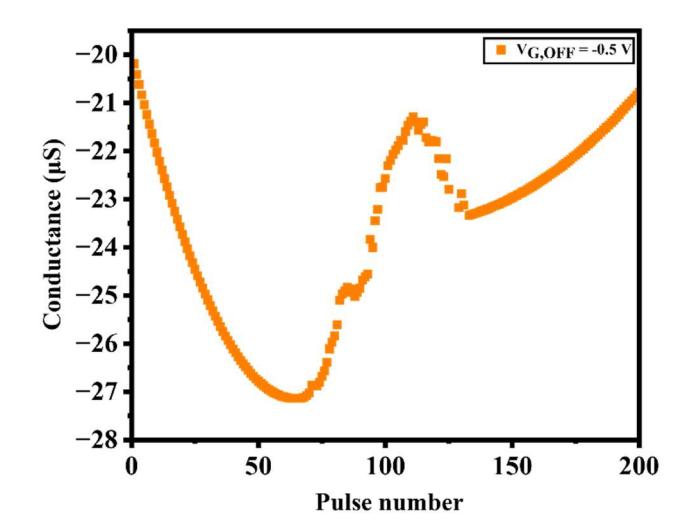
In the above figures, the device shows significant features like biological synaptic system. Depending on action potential stimuli the biological neuron system shows long-term behaviour and short-term behaviour. Similarly, our artificial synaptic device shows the long-term and short-term behaviour like biological neuron system. When the conductance increases with the time and pulse number, the device shows long-term potentiation (LTP) and similarly, the conductance decreases with the time and pulse number, the device shows short-term potentiation (STP). Our device shows significant long-term behaviour at mainly 1.5 V and 2 V. With increasing gate on voltage, our device efficiency also increases. At 0.5 V and 1 V gate on voltage, our synaptic device shows the mixed behaviour. Depending on action stimuli or gate on voltage, our device shows short term and long-term behaviour like human neuron system.

The experiment was done at pulse mode. The three terminal of the device was connected to the keithley instrument by the bread board. The experiment was done at constant drain voltage 0.5 V. The experiment was carried out at same gate on voltage $(V_{G, ON})$ 2 V and different gate off voltage.

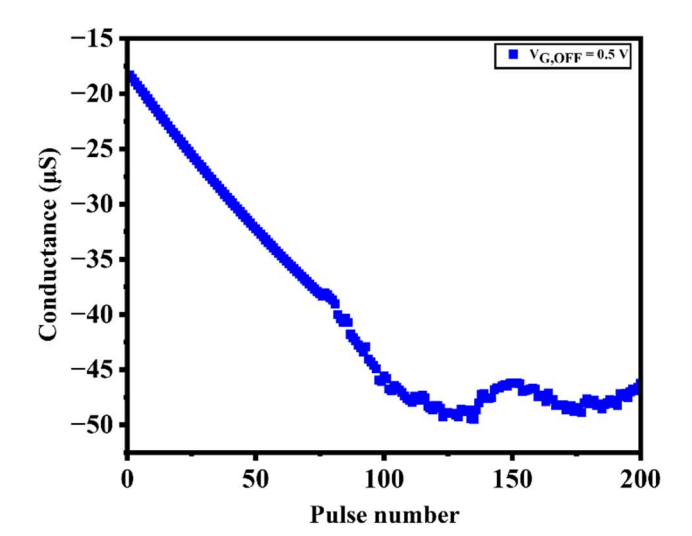
(a)



(b)



(c)



(d)

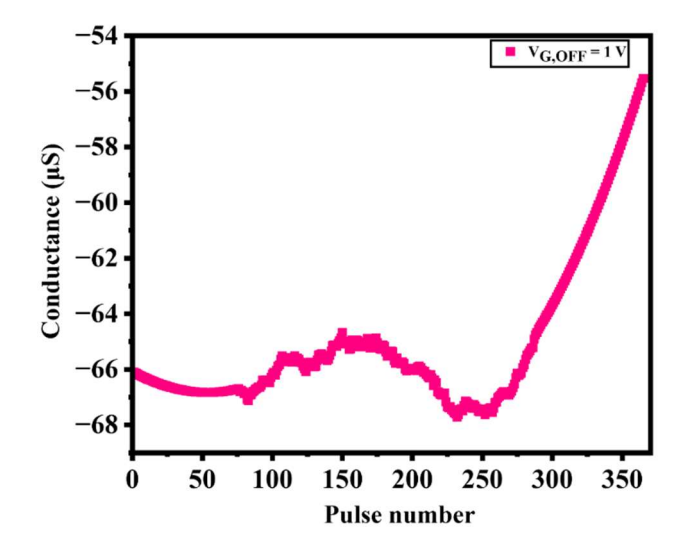


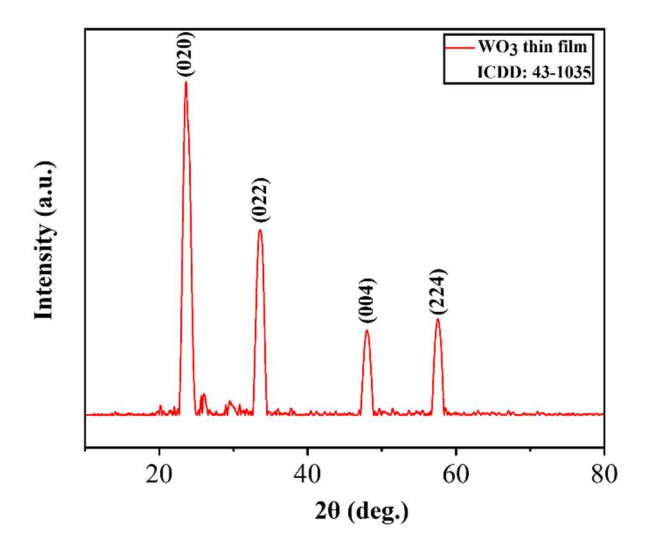
Figure 26: Potentiation–depression curves of synaptic device at constant drain voltage $(V_D) = 0.5 \text{ V}$ and at same on gate voltage $(V_{G, ON}) = 2 \text{ V}$, at $V_{G, OFF}$ voltage (a) -1 V (b) -0.5 V (c) 0.5 V (d) 1 V respectively.

In the experiment, the width of the pulse was 1 MS and the off time of the pulse was 2 S. All the experiment carried out at 0.5 Hz frequency. In all the graph, the device shows the short term and long-term behaviour also. When the gate off voltage was decreases, the conduction of the device was also decreased. This implies that at lower off voltage our device shows short term behaviour. At higher gate off voltage in fig-26(d) at 1 V, our device shows long term potentiation.

5.4 Characterization of WO₃ film on LICGC:

The morphology and composition of the film after annealing was investigated by FE-SEM and AFM analysis. The phase of the film was confirmed by the XRD analysis. The film thickness was ~100 nm. Raman Spectroscopy was used to confirm the formation of tungsten oxide thin film.

(a)



(b)

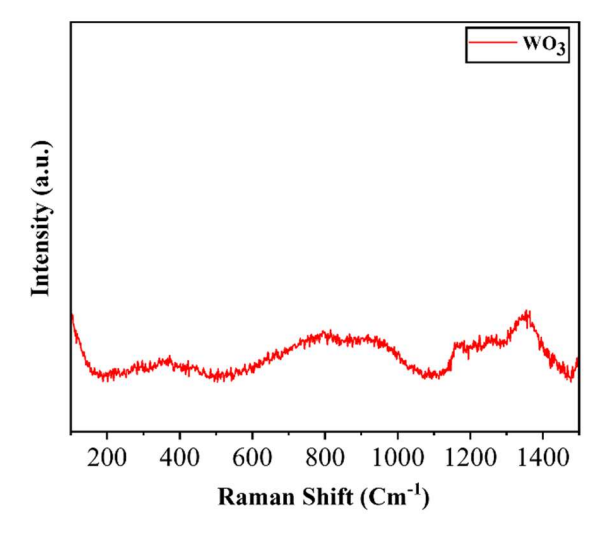


Figure 27: (a) The XRD data of deposited WO₃ film on LICGC (b) The Raman data of deposited WO₃ thin film on LICGC substrate.

The XRD pattern shows clear peaks corresponding to monoclinic WO₃, matching with ICDD PDF 43-1035. Annealing at 450 °C likely improved

crystallinity and facilitated the formation of the thermodynamically stable monoclinic phase. Raman scattering spectra of WO₃ thin film sample are reported in figure 27(b). In raman spectra data of WO₃ film include three main broad bands at 300–500, 600–950, and 1100–1400 cm⁻¹. In crystalline tungsten trioxide, the band at about 950 cm⁻¹ appears as a relatively sharp peak and is ascribed to the stretching mode of the terminal W=O double bond [41].

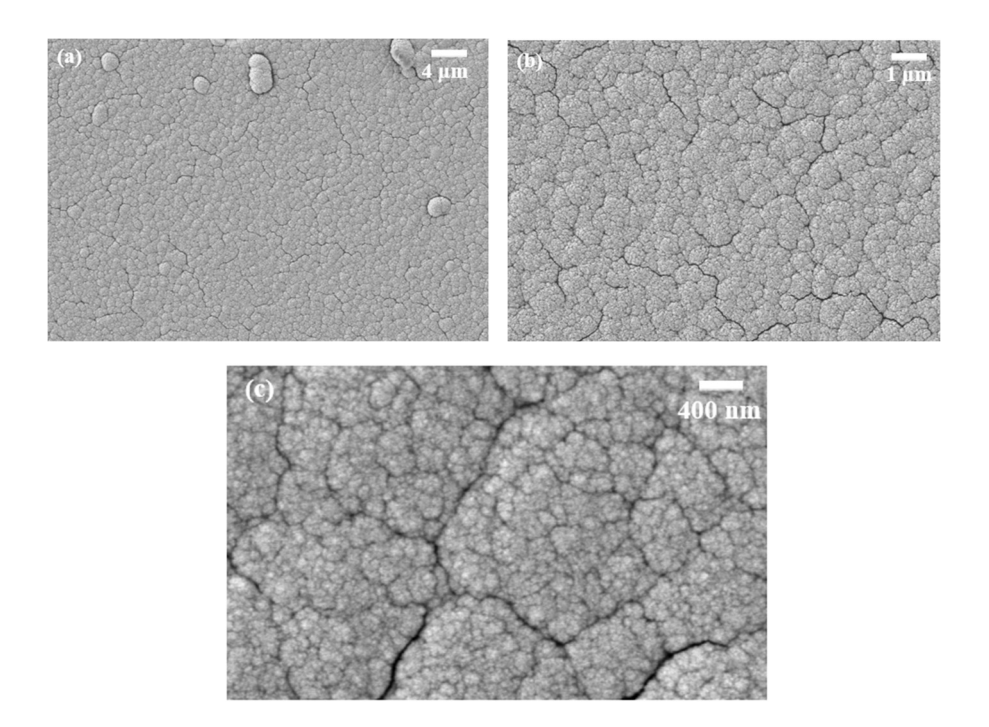


Figure 28: FE-SEM micrographs for the deposited WO₃ film on LICGC substrate at (a) 2.04 KX(b) 5.49 KX (c) 20.33 KX magnification.

From the SEM images we concluded that the film appears to have a granular morphology with relatively uniformly distributed grains. Grain boundaries are distinguishable, suggesting partial crystallization or grain coalescence due to thermal treatment. The observed grain structure indicates that the film has undergone crystallization, typical for WO₃ at this annealing temperature. There was no visible amorphous phase; the grains show faceted edges indicative of crystalline nature. The film appears dense and adherent, with no obvious signs of delamination or micro-cracking.

Minimal porosity and few pinholes, suggesting good film integrity postannealing.

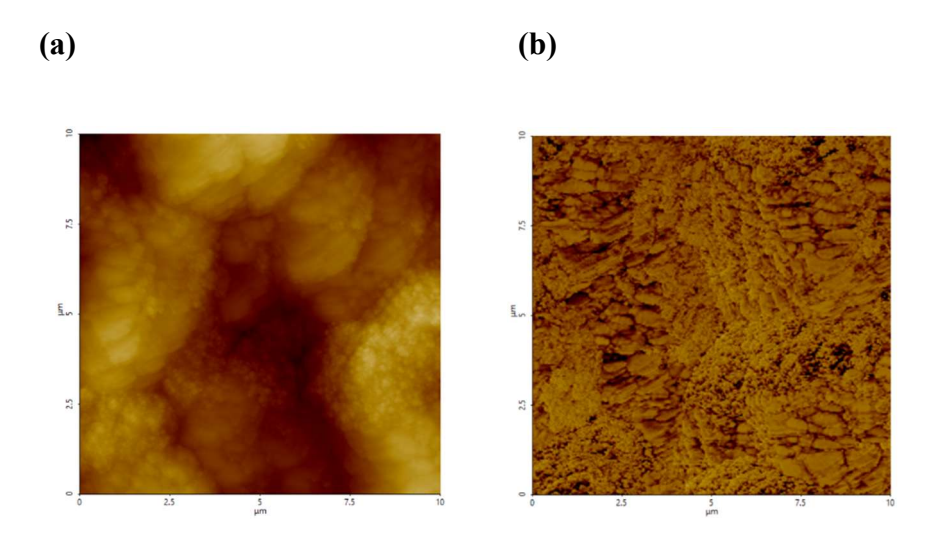


Figure 29: AFM images of the film taken in a 10x10 micron area taken in (a) 0.5 Hz scan rate (b) 1 Hz scan rate.

5.5 Gas sensing mechanism:

When LICGC deposited on WO₃ then, the depletion region is formed at the interface of solid electrolyte and metal oxide surface as shown in figure 30 [42]. Semiconducting metal oxide-based gas sensors are chemiresistive, i.e., resistance will be changed by gas absorption. When oxygen molecules are exposed to air, Oxygen molecules interact with electrons which are present in conduction band of semiconductor metal oxide to form absorbed oxygen or oxide ion. So, the electrons will decrease and the thick depletion region is formed at the surface. Hence, resistance increases and conduction decreases due to thick depletion region. When ethylene gas is introduced into picture, the absorbed oxygen or oxide ion reacts with ethylene gas to form acetaldehyde and electron is returned to conduction band of semiconductor metal oxide. Hence, the thickness of depletion region decreases and the resistance also decreases. So, conduction increases. The response of gas sensor device also increases.

$$C_2H_4(ads) + O^-(ads) \rightarrow C_2H_4O + e^-$$

 $C_2H_4O + 5O^-(ads) \rightarrow 2CO_2 + 2H_2O + 5e^-$

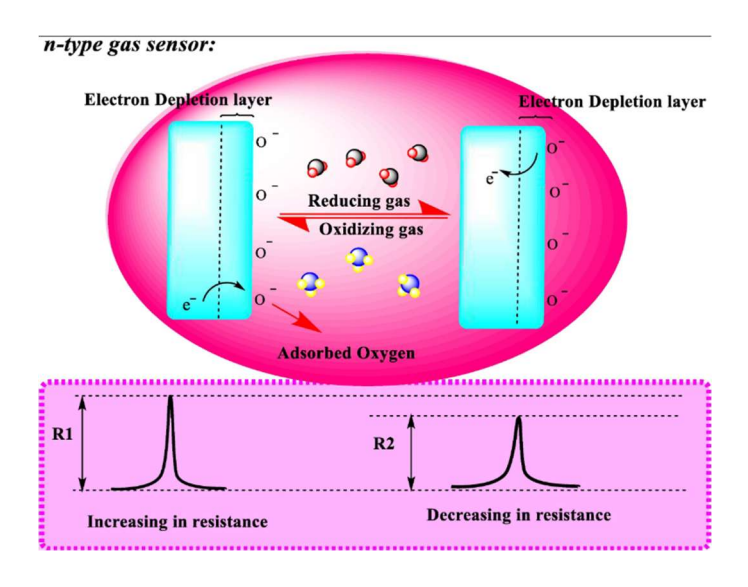


Figure 30: A schematic representation of an n-type chemiresistor gas sensor ^[42].

Chapter 6: Conclusion

In this thesis, we have been successfully fabricated WO₃ based LICGC gas sensor device and we also checked the device efficiency in the presence of ethylene gas. The different operating temperature was used for the gas sensing experiment. The sensor response of the device was also checked at different temperatures. The gas sesing device showed higher response at 170 °C. The gas sensing experiment was also successfully done in pulse mode at room temperature. We also checked the impact of doping on its characteristics. We have used in-situ doping into WO₃ to modify the Li-ion concentration via solid state ionics. The sensor's effectiveness has been demonstrated through tests ethylene gas. We also successfully made the artificial synaptic based ionic decision maker device that showed the biological synaptic behaviours like short-term potentiation/depression and long-term potentiation/depression. We also prepared the LLZO pellet as solid electrolyte for gas sensing device. We also polished the LLZO pellet but the pellet was broken. The characterization of LLZO powder was also done. The WO₃ thin film was successfully characterized by XRD, Raman, FE-SEM and AFM data.

Chapter 7: Future Scope

Experiments will be carried out to model the interfaces and bulk region with an equivalent circuit fitting using electrochemical impedance spectroscopy (EIS). Also, optimization of working temperature will be done so that the sensor can detect lower limits of gas concentration without the need to reach very high temperatures. Such a device can be used in agricultural sector for simple detection of ethylene gas and reduce food spoilage. Sensors embedded in packaging or storage environments can provide real-time ethylene data, improving the freshness of fruits and vegetables while they are being stored and transported. Enhanced ethylene sensors could play a critical role in plant physiology research, providing deeper insights into plant signaling and responses to environmental stimuli. Ethylene is also produced in the human body in certain metabolic pathways. Future research might explore the use of ethylene sensors for medical diagnostics or monitoring specific health conditions. These scopes suggest that ethylene gas sensing will continue to play a crucial role across multiple industries, from agriculture to environmental monitoring and AI-driven smart systems. The future scope of my second project is to further study of the decisionmaking device and how it is connected to our human neuromorphic network system. The correlation will be established in future between decision making device and neural network system in our body. Calcium imaging is important in our body for taking decision in our brain and the correlation between different neurons and synapses. Further scope is to study between calcium imaging and ionic decision-making device.

References

- 1. Tsagarakis, E. The Etymology of Ionics. *Ionics* **2003**, 9, VII-XII.
- 2. Dai, S.; Liu, X.; Liu, Y.; Xu, Y.; Zhang, J.; Wu, Y.; Cheng, P.; Xiong, L.; Huang., J. Emerging Iontronic Neural Devices for Neuromorphic Sensory Computing. *Adv. Mater* **2023**, 35, 2300329(1-29).
- 3. Manikandan, J.; Tsuchiya, T.; Takayanagi, M.; Kawamura, K.; Higuchi, T.; Terabe, K.; Rayavel, R.; Substrate effect on the neuromorphic function of nanoionics-based transistors fabricated using WO₃ thin film. *Solid State Ionics* **2021**, 364, 115638.
- 4. Terabe, K.; Tsuchiya, T.; Tsuruoka, T. Solid state ionics for the development of artificial intelligence components. *Japanese Journal of Applied Physics* **2022**, 61, SM0803.
- 5. Terabe, K.; Tsuchiya, T.; Tsuruoka, T.; Solid state ionics for the development of artificial intelligence components. *Japanese Journal of Applied Physics* **2022**, 61, SM0803.
- 6. Zhao, W.; Yi, J.; He, P.; Zhou, H. Solid-State Electrolytes for Lithium-Ion batteries: Fundamentals, challenges and Perspectives. *Electrochemical Energy Reviews* **2019**, *2* (4), 574–605.
- 7. Zhaoa, Q.; Duana, Z.; Yuana, Z.; Lib, X.; Wanga, S.; Liua, B.; Zhanga, Y.; Jianga, Y.; Taia, h. High performance ethylene sensor based on palladium-loaded tin oxide: Application in fruit quality detection. *Chinese Chemical Letters* **2020**, 31, 2045-2049.
- 8. Leangtanom, P.; Wisitsoraat, A.; Jaruwongrungsee, K.; Chanlek, N.; Phanichphant, S.; Kruefu, V. Highly sensitive and selective ethylene gas sensors based on CeOx-SnO2 nanocomposites prepared by a Coprecipitation method. *Materials Chemistry and Physics* **2020**, *254*, 123540.

- 9. Caprioli, F.; Quercia, L. Ethylene Detection Methods in Post-Harvest Technology: A Review. *Sens Actuators B Chem* **2014**, 203, 187–196.
- 10. Reddy, P. R. S. Advancements in artificial synapses: The role of fluorite-structured ferroelectrics. *Nano Trends* **2025**, *9*, 100074.
- 11. Liu, X.; Sun, C.; Ye, X.; Zhu, X.; Hu, C.; Tan, H.; He, S.; Shao, M.; Li, R. Neuromorphic Nanoionics for Human–Machine Interaction: From Materials to applications. *Advanced Materials* **2024**, *36* (37).
- 12. Kuzum, D.; Yu, S.; Wong, H.P. Synaptic electronics: Materials, devices and applications. *Nanotechnology* **2013**, 24, 382001.
- 13. Liu, S.; Cheng, Z.; Li, M.-Y.; Liu, S.; Lu, H.; Wen, X.; Wang, C.; Ding, X.; Wang, L. Synapses based on lead-free perovskite in artificial intelligence. *Matter* **2024**, *7* (9), 2810–2825.
- 14. Z. Lei.; P. Wu. Short-term plasticity, multimodal memory, and logical responses mimicked in stretchable hydrogels. *Matter* **2023**, 6, 429.
- 15. Reddy, P. R. S. Advancements in artificial synapses: The role of fluorite-structured ferroelectrics. *Nano Trends* **2025**, *9*, 100074.
- 16. Whittle, P. Multi-armed bandits and the Gittins index. *Journal of the Royal Statistical Society B* **1980**, 42, 143–149.
- 17. Dzhoha, A.; Rozora, I.; Multi-armed bandit problem with online clustering as side information. *Journal of Computational and Applied Mathematics* **2023**, 427, 115132.
- 18. Kitagawa, Y.; Tsuchiya, T.; Etoh, D.; Takayanagi, M.; Namiki, W.; Higuchi, T.; Terabe, K. A graphene oxide-based ionic decision-maker for simple fabrication and stable operation. *Japanese Journal of Applied Physics* **2020**, *59* (SI), SIIG03.

- 19. Lin, H.; Wang, J.; Xu, S.; Zhank, Q.; Cheng, Y.; Han, D.; Wang, H.; Zhuo, K. Au-WO₃ Nanowire-Based Electrodes for NO₂ Sensing. *ACS Appl. Nano Mater* **2022**, 5, 14311–14319.
- 20. Tsuchiya, T.; Tsuruoka, T.; Kim, S.J.; Terabe, K.; Aono, M. Ionic decision-maker created as novel, solid-state devices. *Sci. Adv* **2018**, 4, 2057.
- 21. Ohno, T.; Hasegawa, T.; Tsuruoka, T.; Terabe, K.; Gimzewski, J.K.; Aono, M. Short-term plasticity and long-term potentiation mimicked in single inorganic synapses. *Nat. Mater* **2011**, 10, 591–595.
- 22. Yang, R.; Terabe, K.; Liu, G.; Tsuruoka, T.; Hasegawa, T.; Gimzewski, J.K.; Aono, M. On-demand nanodevice with electrical and neuromorphic multifunction realized by local ion migration. *ACS Nano* **2012**, *6*, 9515–9521.
- 23. Park, C.O.; Fergus, J.W.; Miura, N.; Park, J.; Choi, A. Solid-state electrochemical gas sensors. *Ionics* **2009**, 15, 261-284.
- 24. Sholehah, A.; Karmala, K.; Huda, N.; Utari, L.; Septiani, N.L.W.; Yuliarto, B. Structural effect of ZnO-Ag chemoresistive sensor on flexible substrate for ethylene gas detection. *Sensors and Actuators A: Physical* **2021**, 331, 112934.
- 25. Zhang, G.; Liu, M. Effect of particle size and dopant on properties of SnO₂-based gas sensors. *Sensors and Actuators B: Chemical* **2000**, 69(1-2), 144-152.
- 26. Chen, X.; Wreyford, R.; Nasiri, N. Recent Advances in Ethylene Gas Detection. *Materials* **2022**, 15(17), 5813.
- 27. Williams, R.S. How we found the missing memristor. *IEEE spectrum* **2008**, 45(12), 28-35.
- 28. Mathew, R.; Das, A. 2022. Recent advances in ZnO based electrochemical ethylene gas sensors for evaluation of fruit maturity.

- Advanced Functional Materials and Devices: Select Proceedings of AFMD 2021, 213-225.
- 29. Agarwal, M.; Balachandran, M.D.; Shrestha, S.; Varahramyan, K. SnO₂ nanoparticle-based passive capacitive sensor for ethylene detection. *Journal of Nanomaterials* **2012**, 5.
- 30. Shepelin, N.A.; Tehrani, Z.P.; Ohannessian, N.; Schneider, C.W.; Pergolesi, D.; Lippert, T. A practical guide to pulsed laser deposition. *Chemical Society Reviews* **2023**.
- 31. Kwon, T.; Ohnishi, T.; Mitsuishi, K.; Ozawa, T.C.; Takada, K. Synthesis of LiCoO₂ epitaxial thin films using a sol–gel method. *Journal of Power Sources* **2015**, 274, 417-423.
- 32. Berni, A.; Mennig, M; Schmidt, H. Doctor blade (89-92). Springer US **2004**.
- 33. Wang, Z. Q.; Xu, H. Y.; Li, X. H.; Yu, H.; Liu, Y. C.; Zhu, X. J. Synaptic learning and memory functions achieved using oxygen ion Migration/Diffusion in an amorphous InGaZnO memristor. *Advanced Functional Materials* **2012**, *22* (13), 2759–2765.
- 34. Strukov, D. B.; Snider, G. S.; Stewart, D. R.; Williams, R. S. The missing memristor found. *Nature* **2008**, *453* (7191), 80–83.
- 35. Sun, Y.; Li, J.; Li, S.; Jiang, Y.; Wan, E.; Zhang, J.; Shi, Y.; Pan, L. Advanced synaptic devices and their applications in biomimetic sensory neural system. *Chip* **2022**, *2* (1), 100031.
- 36. Das, A.; Sahu, S.; Mohapatra, M.; Verma, S.; Bhattacharyya, A. J.; Basu, S. Lithium-ion conductive glass-ceramic electrolytes enable safe and practical Li batteries. *Materials Today Energy* **2022**, 29, 101118.

- 37. Munir, Z. A.; Quach, D. V.; Ohyanagi, M. Electric Current Activation of sintering: A review of the pulsed electric current sintering process. *Journal of the American Ceramic Society* **2010**, 94 (1), 1–19.
- 38. Raj, R.; Cologna, M.; Francis, J. S. C. Influence of externally imposed and internally generated electrical fields on grain growth, diffusional creep, sintering and related phenomena in ceramics. *Journal of the American Ceramic Society* **2011**, *94* (7), 1941–1965.
- 39. Polyakov, B.; Butanovs, E.; Ogurcovs, A.; Sarakovskis, A.; Zubkins, M.; Bikse, L.; Gabrusenoks, J.; Vlassov, S.; Kuzmin, A.; Purans, J. Unraveling the structure and properties of layered and mixed ReO₃–WO₃ thin films deposited by reactive DC magnetron sputtering. *ACS Omega* **2022**, *7* (2), 1827–1837.
- 40. Hu, Z.; Liu, H.; Ruan, H.; Hu, R.; Su, Y.; Zhang, L. High Li-ion conductivity of Al-doped Li₇La₃Zr₂O₁₂ synthesized by solid-state reaction. *Ceramics International* **2016**, 42 (10), 12156–12160.
- 41. Daniel, M. F.; Desbat, B.; Lassegues, J. C.; Gerand, B.; Figlarz, M. Infrared and Raman Study of WO₃ Tungsten Trioxides and WO₃, XH₂O Tungsten Trioxide Hydrates. *J. Solid State Chem* **1987**, 67, 235–247.
- 42. Najafi, P.; Ghaemi, A. Chemiresistor gas sensors: Design, Challenges, and Strategies: A comprehensive review. *Chemical Engineering Journal* **2024**, *498*, 154999.